OCEANIC LITHOSPHERE AND ASTHENOSPHERE:

THERMAL AND MECHANICAL STRUCTURE

G. Schubert

Department of Geophysics and Space Physics

University of California

Los Angeles, California 90024

C. Froidevaux

Laboratoire de Physique des Solides*

Universite de Paris - Sud

Orsay, France 91405

D. A. Yuen

Department of Geophysics and Space Physics

University of California

Los Angeles, California 90024

*Laboratoire associé an C.N.R.S.
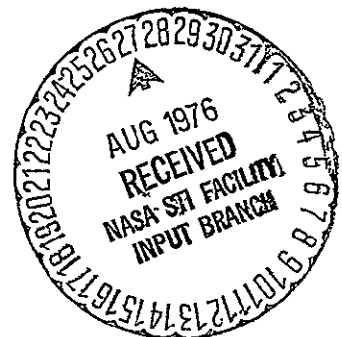
ABSTRACT

We present a coupled thermal and mechanical solid state model of the oceanic lithosphere and asthenosphere which includes vertical conduction of heat with a temperature-dependent thermal conductivity $k(T)$, horizontal and vertical advection of heat, viscous dissipation or shear heating, and linear or nonlinear deformation mechanisms with temperature and pressure-dependent constitutive relations between shear stress and strain rate. A priori assumptions and inputs to the model are relatively few. We require a constant horizontal velocity u_o and temperature T_o at the surface and zero horizontal velocity and constant temperature T_∞ at great depth. In addition to numerical values of the thermal and mechanical properties of the medium, we specify only the values of u_o, T_o and T_∞. The model determines the depth and age-dependent temperature, horizontal and vertical velocity, and viscosity structures of the lithosphere and asthenosphere. In particular, we deduce therefrom ocean floor topography, oceanic heat flow, and lithosphere thickness as functions of the age of the ocean floor. The model also yields the age-dependent shear stress in the lithosphere and asthenosphere. From the age-dependent geotherms and assumed values of the elastic parameters we construct seismic velocity profiles which exhibit a marked low velocity zone. To a first approximation, simple boundary layer cooling, i.e. the growth of

a cold thermal boundary layer by upward conduction of heat with $k(T)$ and horizontal advection of heat with constant velocity u_o, determines the thermal structure and quantities derivable essentially solely therefrom, namely oceanic heat flow, ocean floor topography, and seismic velocities. The simple boundary layer cooling solution gives heat flow $\propto (age)^{-\frac{1}{2}}$ and depth of the ocean $\propto (age)^{\frac{1}{2}}$, for example. The second approximation, i.e. the self-consistent thermo-mechanical solution, provides modifications to the thermal structure associated with shear heating effects. This solution also gives the horizontal and vertical velocity, and viscosity structures not determined by simple boundary layer cooling and such quantities as the age-dependent lithosphere and asthenosphere thicknesses derivable from the mechanical field. Effects of viscous dissipation at old ages tend to flatten heat flow, ocean depth and lithosphere thickness vs. age curves, e.g. although ocean depth and lithosphere thickness tend to increase with age at all ages, shear heating tends to reduce the rate of increase at old ages below that given by $(age)^{\frac{1}{2}}$. The importance of shear heating increases with plate velocity, decreases with subasthenospheric temperature T_∞, increases with the activation volume describing the pressure-dependence of viscosity, and increases with age of the ocean floor.

INTRODUCTION

The history of the ocean floor is now well documented
from magnetic anomaly and deep sea drilling studies. It is
generally acknowledged that geophysical characteristics like
topography and heat flow are essentially a function of the
age of the ocean floor and, therefore, are practically
identical for a slow spreading ocean, the Atlantic, and a
fast spreading ocean, the Pacific (Sclater and Francheteau,
1970). This universal dependence on age is particularly
striking for topography, whereas heat flow data are now
known to be affected by hydrothermal circulation in the
young oceanic crust so that the scatter in heat flow values
is large and the average values of heat flow by conduction
do not represent the entire heat flow to the surface (Lister,1972,
1974). For the Pacific ocean, the depths of the seismic
low velocity channel for various ages are also available
(Kausel et al., 1974).

Physical models of the oceanic upper mantle providing
a basic understanding of the geophysical data are derived
from either the boundary layer cooling of a convective cell
(Turcotte and Oxburgh, 1967) or from the cooling of a rigid
slab of fixed thickness moving at constant velocity away
from a hot vertical boundary (McKenzie, 1967). The simple
boundary layer cooling model leads to a $\sqrt{age}$ proportionality

for quantities like depth of the ocean floor, inverse of surface heat flow, or depth to a given isotherm. For young ages, these proportionalities are also predicted by the rigid slab cooling model. Davis and Lister (1974) have in fact shown that ocean floor topography data for 0-80 My plot on a straight line vs. $\sqrt{age}$. For ages larger than its thermal conduction time the constant thickness slab model of course shows departures from this simple behavior (Parsons and Sclater, 1976). These authors have presented new topographic data corresponding to zero free air gravity anomalies for the North Atlantic and for the North Pacific extending to 100 My and 145 My, respectively. The topographic data depart from a simple $\sqrt{age}$ law for the oldest parts of the ocean floor. There is also a suggestion in the heat flow data of a flattening in the heat flux at great age (Sclater et al., 1976).

These purely thermal models give, of course, no information about the mechanical structure of the upper mantle, i.e. about the geometry of the lithosphere and asthenosphere and about the velocity field. A lithospheric thickness can however be defined if the assumption is made that a given isotherm, say 1200 $^{\circ}$C, marks the transition between a solid lithosphere and an asthenosphere where partial melting generally occurs. This approach is based on a widespread belief that the seismic low velocity zone, which is well developed under oceanic regions, but not under old continental shields (Knopoff, 1972), corresponds to the occurrence of temperatures exceeding the solidus of

mantle material (Anderson and Sammis, 1970).

In this spirit Parker and Oldenburg (1973) have cal-
culated a lithospheric thickness proportional to $\sqrt{age}$.
It should be stressed that this definition of the lith-
osphere-asthenosphere boundary is different from that of
plate tectonics which defines the asthenosphere as a zone
of mechanical decoupling of the plates from the lower mantle.
Furthermore, mechanisms other than partial melting may
generally account for the zone of low velocity and high
attenuation of seismic waves (Gueguen and Mercier, 1972).
It is however often assumed that this zone of low velocity
corresponds roughly with the asthenosphere in the mechan-
ical sense. Physically, this coincidence could be correct
since high temperatures can favor both dissipative phenomena
(wave attenuation, shear deformation) and decrease of elastic
moduli (wave velocities). It is however not required that
partial melting occur to have viscosities low enough to
account for lithospheric decoupling. Ample laboratory
data on the plastic deformation of olivine at high tem-
perature and pressure have confirmed this (Post, 1973;
Kohlstedt and Goetze, 1974).

In this paper we investigate both the thermal and
mechanical structures of the oceanic upper mantle. Thermal
quantities and associated topographic effects are computed
simultaneously with mechanical quantities such as velocity
and shear stress. Non-Newtonian and Newtonian rheological
laws are used. We shall see that we account for available

geophysical data, in particular, for departures from a simple proportionality with $\sqrt{age}$. Experimental values are used for the material properties so that in principle the model contains no adjustable parameters. Our results should help to formulate new geophysical programs aimed at a better understanding of the dynamic structure of tectonic plates.

QUALITATIVE DESCRIPTION OF THE MODEL

The thermal and mechanical structures of the oceanic lithosphere and asthenosphere are coupled via the contribution of shear heating to the temperature distribution and the dependence of viscosity on temperature. Aside from the work of Schubert and Turcotte (1972), we are unaware of investigators who have considered this coupled thermo-mechanical problem; the point of view in most modelling efforts has been to consider the material beneath the ocean floor to move horizontally with the constant velocity u_o and to solve the temperature equation by including horizontal advection of heat and upward conduction of heat (Langseth et al., 1966; McKenzie, 1967; Turcotte and Oxburgh, 1967). In this paper we develop a theory for the coupled thermo-mechanical characteristics of the oceanic lithosphere and asthenosphere which includes important phenomena heretofore largely neglected in the modelling of these suboceanic structures.

The model we consider is sketched in Figure 1. Material rising from beneath the ridge moves essentially horizontally away from the ridge, cooling to the surface as it ages. The cooling results in the formation of a boundary layer or lithosphere which is essentially rigid and moves with the horizontal velocity of the surface u_o. Beneath the lithosphere is the asthenosphere, a region wherein the mantle material is sheared and the horizontal velocity is reduced to zero. Within the asthenosphere there is also

a small upward velocity v to supply the mass required by the thickening, horizontally moving lithosphere. The upward asthenospheric flow must be supplied by a deeper mantle circulation not considered here.

On the left side of Figure 1 we list the quantities we input to our model. At the surface, we specify the temperature $T = T_o$, the horizontal velocity $u = u_o$ and the vertical velocity $v = 0$. At great depth we require the temperature to rise to a constant value T_∞ and the horizontal velocity to be zero. The T_∞ boundary condition facilitates comparison with the simple boundary layer cooling solution. The right hand side of the figure shows the information we extract from the model calculations. This includes temperature, horizontal velocity, vertical velocity, shear stress, viscosity, and seismic velocities as functions of depth y and distance from the ridge x (or age $= x/u_o$). From the thermal structure of the suboceanic mantle we also infer the topography of the ocean floor and surface heat flow as a function of age.

Our model includes the following features:

1. Conduction of heat in the vertical.

2. Thermal conductivity that depends on temperature.

3. Advection of heat by a horizontal and vertical mass flow that depends on depth and age; the depth and age dependent vertical flow supplies the lithospheric mass.

4. Contribution of viscous dissipation or shear heating to the thermal state.

5. Linear or nonlinear deformation law relating shear stress and strain rate.

6. Temperature and pressure dependent viscosity.

We derive the structure of the oceanic lithosphere
and asthenosphere simply on the basis of subsolidus effects.
This point of view contrasts with that of Parker and
Oldenburg (1973) and Oldenburg (1975), who define the base
of the lithosphere as a solid-liquid phase boundary.

As in our model of the continental asthenosphere
(Froidevaux and Schubert, 1975) the shear stress will be
found to take a nonzero value at the surface of the plate
(y = 0). This artificial stress at the surface replaces
the driving forces acting, for example, at the plate boun-
daries. Elsasser (19 69) has pointed out that the lithosphere
may act as a stress guide. Our surface shear stress repre-
sents this phenomenon. Its magnitude is not pre-determined.
What is imposed is the surface velocity.

MATHEMATICAL FORMULATION

As described in the preceding section, the suboceanic litho-
sphere can be viewed as the relatively cold, near surface ther-
mal boundary layer of a convecting mantle. As material spreads
from an oceanic ridge, cooling to the surface occurs, resulting
in the formation of the thermal boundary layer or lithosphere;
the boundary layer thickens with increased distance from the
spreading center, i.e. with age of the lithosphere. The sit-
uation has been sketched in Figure 1.

Constant Thermal Conductivity and Horizontal Velocity

The simplest mathematical description of the temperature
profile in the oceanic upper mantle away from the ridge axis ex-
presses a balance between conduction of heat vertically and advec-
tion of heat horizontally at a constant lithospheric velocity u_o

$$\rho c_p u_o \frac{\partial T}{\partial x} = \bar{k} \frac{\partial^2 T}{\partial y^2} \tag{1}$$

where ρ is the lithospheric density, c_p is the specific heat at
constant pressure, $\bar{k}$ is the thermal conductivity, x is the hori-
zontal distance from the ridge, y is the depth and T is the tem-
perature. In writing the boundary layer equation (1) we have
assumed $\frac{\partial}{\partial x} << \frac{\partial}{\partial y}$ (i.e. vertical heat conduction is much more im-
portant than horizontal conduction of heat) and ρ, c_p, u_o and $\bar{k}$
are constants. This boundary layer approach is not valid very close
to the ridge. It is an accurate description as long as the combined
thickness of the lithosphere and asthenosphere is small compared with
the distance from the ridge. Equation (1) is solved subject
to the conditions that at the surface,

$y = 0$, T is equal to T_o and at greath depth, $y \to \infty$, T tends to T_∞ (a constant).

The solution of (1), obtained by Turcotte and Oxburgh (1972), is

$$T = T_o + (T_\infty - T_o) \, \mathrm{erf}\{\frac{y}{2}(\frac{\rho u_o c_p}{\overline{k}x})^{\frac{1}{2}}\} \qquad , \qquad (2)$$

where erf is the error function. The surface heat flux q_o (positive upwards) associated with this temperature distribution is

$$q_o = \overline{k} \, \frac{\partial T}{\partial y}(y=0) = \overline{k}(T_\infty - T_o)(\frac{\rho u_o c_p}{\pi \overline{k} x})^{\frac{1}{2}} \qquad . \qquad (3)$$

As shown in (2), the temperature depends on x and y in the combination $y/\sqrt{x}$. Surface heat flow decreases as $x^{-\frac{1}{2}}$ or (age)$^{-\frac{1}{2}}$ and the "thickness" of the lithosphere grows as $\sqrt{x}$ or (age)$^{\frac{1}{2}}$, if lithospheric thickness can be defined as the depth to a particular isotherm.

As the relatively cold lithosphere thickens with age, it contracts, and the weight of a vertical column of rock of constant height also increases with age. If we require isostasy, then the thermal contraction of the aging lithosphere is reflected in the bathymetry, i.e. the depth of the ocean floor must increase with age. By accounting for the bathymetry of the ocean floor and the thermal contraction of the rocks with age, one finds equal masses in vertical columns of rock and seawater if

$$D = D_{ref} - \frac{\alpha}{(1 - \frac{\rho_{sw}}{\rho})} \int_0^{\infty} dy\, (T - T_{ref}) \qquad , \qquad (4)$$

where D is the depth of the ocean floor, α is the thermal expansivity, ρ_{sw} is the density of seawater and the subscript ref indicates a reference condition, i.e. D_{ref} and T_{ref} are the depth and temperature at a particular age of the ocean floor. In evaluating (4), one may assume ρ is a constant. With the temperature profile (2), we can integrate (4) analytically to obtain

$$D = D_{ref} - \frac{2\alpha(T_{\infty} - T_0)}{(1 - \frac{\rho_{sw}}{\rho_{\infty}})} \sqrt{\frac{\bar{\kappa}}{\pi}} \left(\sqrt{\frac{x_{ref}}{u_0}} - \sqrt{\frac{x}{u_0}} \right) , \qquad (5)$$

where $\bar{\kappa}$, the thermal diffusivity, is $\bar{k}/(\rho c_p)$. Thus the depth of the ocean floor also increases as $\sqrt{x}$ or $\sqrt{age}$.

This solution provides an adequate zeroth order description of the temperature in the oceanic lithosphere. It does not, however, include the effects of a variable thermal conductivity, advection by a more realistic flow field and the viscous dissipation of the flow. Moreover, we have learned nothing about the structure of the velocity in the oceanic asthenosphere since we assumed, a priori, a constant horizontal velocity u_0. In the following, we generalize the solution (2) for the temperature to account for the above-mentioned effects and simultaneously we determine the mechanical structure of the asthenosphere, wherein the horizontal velocity drops from its surface value to zero.

Variable Thermal Conductivity, Constant Horizontal Velocity

First we consider the effect of a thermal conductivity k which is an arbitrary function of temperature. In general, when k is not constant, equation (1) must be replaced by

$$\rho u_o c_p \frac{\partial T}{\partial x} = k \frac{\partial^2 T}{\partial y^2} + \frac{\partial k}{\partial y} \frac{\partial T}{\partial y} \qquad . \qquad (6)$$

In the case k = k(T) we can rewrite (6) as

$$\rho u_o c_p \frac{\partial T}{\partial x} = k \frac{\partial^2 T}{\partial y^2} + (\frac{\partial T}{\partial y})^2 \frac{dk}{dT} \qquad . \qquad (7)$$

This nonlinear equation is essentially no more difficult to solve than (1), the linear equation for constant k, since (7) also possesses a similarity solution.

Let k_o be the value of thermal conductivity at the surface and introduce the similarity variable

$$\xi = \frac{y}{2}\sqrt{\frac{\rho u_o c_p}{k_o x}} \qquad . \qquad (8)$$

The dimensionless temperature

$$\theta = \frac{T - T_o}{T_\infty - T_o} \qquad (9)$$

then has to satisfy the ordinary differential equation

$$-2\xi \frac{d\theta}{d\xi} = (\frac{k}{k_o}) \frac{d^2\theta}{d\xi^2} + (\frac{d\theta}{d\xi})^2 (\frac{d}{d\theta} \frac{k}{k_o}) \qquad (10)$$

and the boundary conditions

$$\theta = 0 \text{ at } \xi = 0 \text{ and } \theta \to 1 \text{ as } \xi \to \infty \qquad . \qquad (11)$$

The upward heat flux q, according to (8) and (9), is given by

$$q = k \frac{\partial T}{\partial y} = \frac{k_o(T_\infty - T_o)}{2} \sqrt{\frac{\rho u_o c_p}{k_o x}} \cdot \frac{k}{k_o} \cdot \frac{d\theta}{d\xi} \qquad , \qquad (12)$$

and the topography of the ocean floor is calculated from (4), (8) and (9). It becomes

$$D = D_{ref} - \frac{2\alpha(T_\infty - T_o)\sqrt{\kappa_o}}{(1 - \frac{\rho_{sw}}{\rho})} \left(\sqrt{\frac{x_{ref}}{u_o}} - \sqrt{\frac{x}{u_o}} \right) \int_o^\infty (1 - \theta(\xi)) d\xi$$

$$. \quad . \qquad (13)$$

Thus heat flux, bathymetry, and lithosphere thickness depend on age in the same manner as they do for constant k; only proportionality factors are modified by variable k.

We have numerically integrated (10) and (11) for the experimental thermal conductivity function of Schatz and Simmons (1972)

$$\frac{k}{k_o} = \frac{88.33}{31 + 0.21T} \qquad \text{for } T < 500 \text{ K}$$

and

$$\frac{k}{k_o} = \frac{88.33}{31 + 0.21T} + 0.486 \times 10^{-3}(T - 500) \qquad \text{for } T > 500 \text{ K}$$

$$(14)$$

where T is in degrees Kelvin and k_o is 0.0113 cal/(cm sec K)
for an assumed surface temperature of 0 ^{o}C.

The solutions show that the conductivity decreases
with ξ for ξ small (conductivity decreases with depth
near the surface) and then increases gradually toward the
value $k(T_\infty)$. For T_∞ = 1200 ^{o}C the minimum value of k/k_o
is about 0.6 at $\xi \approx 0.4$ and the asymptotic value is 0.73.
For T_∞ = 1600 ^{o}C the minimum is also about 0.6 at $\xi \approx 0.5$ and the
asymptotic value is 0.88. Within the upper mantle there
is about a factor of 2 variation in the thermal conductivity.

The surface heat flux from (10) - (12) and (14) is

$$q_o = c_1 k_o (T_\infty - T_o) (\frac{\rho u_o c_p}{k_o x})^{\frac{1}{2}} \tag{15}$$

where c_1 is 0.4656 for T_∞ = 1200 ^{o}C and 0.4680 for T_∞ =
1600 ^{o}C. Since (15) is an exact solution for variable k,
it is not necessary to use (3) together with some estimate
of an average $\bar{k}$ to account for variable conductivity.
Finally, we note that the bathymetry, from (10), (11), (13)
and (14) yields

$$D = D_{ref} - \frac{c_2 (T_\infty - T_o) \alpha \sqrt{k_o}}{(1 - \frac{\rho_{sw}}{\rho})} \left(\sqrt{\frac{x_{ref}}{u_o}} - \sqrt{\frac{x}{u_o}} \right), \tag{16}$$

where c_2 is 0.932 for T_∞ = 1200 ^{o}C and 0.948 for T_∞ =
1600 ^{o}C.

The temperature profiles derived from this similarity
treatment will be shown as reference profiles later on
(see e.g. Figure 4).

Two-Dimensional Shear Flow, Viscous Dissipation, Variable Thermal Conductivity

Exact similarity solutions are no longer possible when one considers the combined thermo-mechanical structure of the oceanic lithosphere and asthenosphere. We formulate instead a quasi-one-dimensional or quasi-similarity approach to the problem which uses the simple boundary layer cooling solutions previously discussed as a starting point. The model, as previously outlined in connection with Figure 1, includes the two-dimensional flow of a medium with a Newtonian or non-Newtonian temperature and pressure dependent rheology forced to deform with horizontal velocity u_o at the surface and zero horizontal velocity at great depth. The depth interval in which there is shear in the horizontal velocity u is the asthenosphere. The asthenosphere is simply a zone of decoupling for the plate; it is not required that a shallow return flow occurs within its depth range. Conservation of mass requires a vertical transport with velocity v to balance the variation in horizontal mass flux due to the change in u(x) with age (x/u_o) or distance from the ridge x. The temperature equation includes advection of heat by both the horizontal and vertical motions, the viscous dissipation of the flow, and variable thermal conductivity.

We are interested in describing the structure of the oceanic lithosphere and asthenosphere which extends over horizontal distances of 1000 - 10,000 km but is only 100 to 300 km thick; thus we have again $y/x \ll 1$ and $\partial/\partial x \ll \partial/\partial y$. With the Boussinesq assumption, conservation of mass is

$$\frac{\partial u}{\partial x} + \frac{\partial v}{\partial y} = 0 \qquad (17)$$

v/u is $0(y/x)$ and $u\frac{\partial}{\partial x}$ is $0(v\frac{\partial}{\partial y})$. These order of magni-tude relationships permit us to write the temperature equation in the approximate form

$$\rho c_p (u\frac{\partial T}{\partial x} + v\frac{\partial T}{\partial y}) = k\frac{\partial^2 T}{\partial y^2} + (\frac{\partial T}{\partial y})^2 \frac{\partial k}{\partial T} + \tau\frac{\partial u}{\partial y} \quad , \qquad (18)$$

where τ is the shear stress acting parallel to a horizon-tal surface element in the medium. The third term on the right hand side of (18) is the dominant contribution to shear stress heating or viscous dissipation.

The rheological law connecting shear stress and strain rate takes the simplified form

$$\frac{\partial u}{\partial y} = - \frac{2B_n}{T} \tau^n \exp\{- \frac{(E^*+pV^*)}{RT}\} \quad , \qquad (19)$$

where E* is the activation energy, V* is the activation volume, p is the pressure, R is the gas constant and B_n is a proportionality factor. For Newtonian flow n = 1 and for non-Newtonian flow n is larger than 1. We will assume in the following that n = 3 for non-Newtonian flow, a value appro-priate for the deformation of olivine. The T^{-1} factor is not re-solved in experiments, but derives from theoretical models of dis-location motions.

If we assume infinite Prandtl number so that the momentum equation expresses a balance between pressure, viscous and gravity forces and further assume zero horizontal pressure gradient, then we may approximate the pressure by its hydro-static value and the horizontal momentum equation becomes

$$\frac{\partial \tau}{\partial y} = 0 \tag{20}$$

We take the horizontal pressure gradient to be zero since
we are mainly interested in the relatively simple case of
asthenospheric decoupling of a rigid moving lithosphere
from a quasi-static deep mantle. A basically horizontal
shear flow can accomplish this decoupling without the
imposition of an external horizontal pressure gradient.
We will consider the effect of a non-zero pressure gradi-
ent in driving a return flow in the oceanic asthenosphere
in a subsequent paper. The boundary conditions for (17) –
(20) are

$$u = u_o, \quad T = T_o, \quad v = 0 \text{ on } y = 0,$$

$$u \to 0, \quad T \to T_\infty \text{ as } y \to \infty \tag{21}$$

Equations (17) – (20) are very similar to the ones
investigated by Froidevaux and Schubert (1975) in their
study of the continental asthenosphere. The equations
for the continental asthenosphere were strictly one-
dimensional, i.e. $v = 0$ and $\frac{\partial}{\partial x} = 0$. However, the cooling
of the oceanic lithosphere as it moves away from the ridge
and ages requires that we include the advective terms on
the left hand side of the temperature equation in our des-
cription of the oceanic asthenosphere. The equations are
also similar to the ones used by Schubert and Turcotte
(1972) in their one-dimensional analysis of a return flow

in the oceanic asthenosphere. Schubert and Turcotte (1972)
did not include the advective terms in the temperature
equation but they partly accounted for lithospheric cool-
ing by integrating the one-dimensional equations with respect
to depth, starting at an a priori specified depth where the
oceanic temperature was assumed to already have risen to a
sufficiently high value, over 800 ^{o}C, that flow readily
occurred, i.e. they began their integration essentially at
the base of the lithosphere whose depth and temperature
were assumed. In this paper, however, we integrate the
equations from the surface of the ocean floor downward
and determine the thermal and mechanical structures of the
oceanic lithosphere and asthenosphere self-consistently.

We solve the system (17) - (21) by a method of successive
approximation which can, in principle, be carried through to
an exact solution of the two-dimensional problem. In the
first step, we assume that the form of the simple boundary
layer cooling solution for the temperature structure of
the lithosphere (henceforth when we refer to simple boundary
layer cooling we mean the case $u \equiv u_o$, $v \equiv 0$ and variable k)
provides a way of relating local horizontal derivatives to
local vertical derivatives. Since boundary layer cooling
with $u \equiv u_o$ and $v \equiv 0$ gives a thermal structure dependent
on y and x, in the combination $y/\sqrt{x}$, we initially take

$$\frac{\partial}{\partial x} = -\frac{1}{2}\frac{y}{x}\frac{\partial}{\partial y} \qquad (22)$$

Then the system (17) - (21) reduces to a set of ordinary non-linear differential equations with y as the independent variable and x as a parameter

$$\frac{y}{2x}\frac{du}{dy} = \frac{dv}{dy} \qquad\qquad , \quad (23)$$

$$\rho c_p (v - \frac{1}{2}\frac{y}{x}u)\frac{dT}{dy} = k\frac{d^2T}{dy^2} + (\frac{dk}{dT})(\frac{dT}{dy})^2 + \tau\frac{du}{dy} , \quad (24)$$

$$\frac{du}{dy} = -\frac{2B_n}{T}\tau^n exp(-\frac{(E^*+pV^*)}{RT}) \qquad , \quad (25)$$

$$\frac{d\tau}{dy} = 0 \qquad\qquad . \quad (26)$$

Because (23) - (26) are coupled equations with the parameter x, their solution subject to conditions (21) will depend on distance from the ridge, i.e. on age. The solution of (21) and (23) - (26) thus provides information on the age dependences of the thermal and mechanical properties of the lithosphere and asthenosphere not assumed a priori. A second approximation can further improve the solution. Instead of replacing $\partial T/\partial x$ and $\partial u/\partial x$ in (17) - (21) by the approximation (22), we can evaluate these derivatives, as functions of x and y, from the solutions of (21) and (23) - (26) since we can obtain these solutions at arbitrarily close values of x. Equations (23) - (26) would then be replaced by a more accurate set of ordinary differential

equations in y. By repeating this process a number of times, a solution of the two-dimensional problem can be obtained to any desired accuracy. In this paper, we obtain the solution to the first approximation only, i.e. we solve (21) and (23) - (26).

Equation (24) contains a second derivative of T; the two boundary conditions on T, namely $T = T_o$ on $y = 0$ and $T \rightarrow T_\infty$ as $y \rightarrow \infty$ are thus sufficient to determine the temperature. Since (23) - (25) contain only first derivatives of velocity, the boundary conditions $u = u_o$ and $v = 0$ on $y = 0$ suffice for the solution of the velocity field. From (26) we know that the shear stress is independent of depth. However, its value is not known a priori and further, it is a function of x. The condition $u \rightarrow 0$ as $y \rightarrow \infty$ is an additional constraint on the solution of (21) and (23) - (26) that serves to determine τ. Thus we not only find the temperature and velocity fields by solving this system, but in addition we solve for the a priori unknown shear stress and its dependence on age. In connection with the age dependence of τ, we note that if the pressure is to be approximated by the lithostatic pressure then

$$\frac{dp}{dy} = 0\,(\rho g) \gg \frac{d\tau}{dx}$$

where g is the acceleration of gravity. That this is an excellent approximation can be seen a posteriori from the solutions for τ.

We will be interested in the profile of viscosity in the asthenosphere and the variation of the viscosity structure with age. Dynamic viscosity η is related to temperature and pressure by

$$\eta \equiv \frac{\tau}{2\dot{\varepsilon}} = \frac{T}{2B_n \tau^{n-1}} \exp(\frac{E^*+pV^*}{RT}) \tag{27}$$

where $\dot{\varepsilon}$ is the strain rate $\frac{-1}{2}\frac{\partial u}{\partial y}$. Note that η depends on τ for $n \neq 1$, i.e. that any viscosity value refers to a given stress level or rate of deformation for non-Newtonian rheologies. One speaks of an effective viscosity for such nonlinear rheologies.

SOLUTIONS TO THE THERMO-MECHANICAL MODEL

Temperature and velocity profiles together with the value of the shear stress have been calculated on the basis of the set of equations and boundary conditions given above and for parameter values enumerated below. This section describes the results both for non-Newtonian and Newtonian rheologies and emphasizes the main chacteristics of verti-cal structure of our model mantle at 2 ages, 10 My and 150 My. The variation of the lithosphere-asthenosphere structure with age will be presented in the next section.

Parameter Values

Our numerical solutions are based on the following values of thermal, mechanical, and kinematic parameters. For the surface temperature T_o we take 0^oC and for the temperature at great depth T_∞ we consider values between 1200 ^oC and 1600 ^oC. We have already noted that the value of thermal conductivity at the surface is 0.01132 cal/cm sec K, while (14) gives the value of k at temperature T. The pressure dependence of k is not included. The specific heat at constant pressure c_p is assumed to be 0.27 cal/(g K) and the density ρ is 3.3 g/cm^3. Thus the value of the thermal diffusivity at the surface temperature, $\kappa_o = \frac{k_o}{\rho c_p}$, is 1.27×10^{-2} cm^2/sec. The coefficient of thermal expansivity α is somewhat uncertain and furthermore is temperature dependent. Its value enters our analysis only in the

calculation of the topography of the ocean floor; we con-
sider averaged values of α between 3×10^{-5} K^{-1} and 4×10^{-5} K^{-1}
(Clark, 1966). To encompass the range of observed plate
velocities in our calculations we take u_o equal to 2 cm/yr
and 10 cm/yr, representative of the North Atlantic and
Pacific oceans, respectively.

The extent to which the simple boundary layer cooling
solutions are modified by two-dimensional shear flow and
viscous dissipation therein depends on the type of rheology
and rheological parameter values assumed for the deforma-
tion. We have investigated both Newtonian (n = 1) and
non-Newtonian (n = 3) rheologies. In each case, two sets
of rheological parameter values were considered, correspond-
ing to materials which deform relatively easily and those
which are relatively harder to shear.

The rheological parameter values are summarized in
Table 1. Since the activation volume V^* is still an un-
certain parameter we have considered it in the range 11-
30 cm^3/mole. It should be noted that the rheological
parameter values for the Newtonian cases are based on
quasi-theoretical estimates. Laboratory results for oli-
vine lead to a nonlinear rheology with n = 3. The olivine
data of Table 1 were not all available when the continen-
tal upper mantle model was investigated (Froidevaux and
Schubert, 1975 (see, in particular, the note added in proof)).
Thus the value of B used here for dry olivine differs from
that used in our earlier paper. Another difference from

our continental model is the absence of both radioactive
heat sources and heat flow from great depth. Such charac-
teristics could be included in future extensions of the
oceanic model.

Temperature Profiles in a Dry Olivine Mantle

We present the solutions of (23) − (26) with boundary
conditions (21) for a number of cases based on the dry
olivine rheological parameter values given in column 1 of
Table 1. The solutions are for two values of u_o, T_∞, and
V* and two different ages.

First we concentrate on the temperature vs. depth
curves for the case $T_\infty = 1600\ ^{\circ}C$. The top of Figure 2
shows two temperature profiles for a plate moving at
2 cm/yr with respect to the lower mantle, one for an age
of 10 My, the other for an age of 150 My. These profiles
are essentially identical to the simple boundary layer
cooling solution (7), so that viscous dissipation is negligi-
ble. This is still nearly the case when the plate velocity
is 10 cm/yr, as illustrated at the bottom of Figure 2.
However, here the 150 My temperature curve, in fact, lies
slightly above the corresponding boundary layer cooling
solution (not shown on the figure), so that the heat flow
at the surface is 1.13 HFU as compared to the boundary
layer cooling result of 1.09 HFU (see Table 2).

Such dissipative effects are more pronounced in Figure 3, which is similar to Figure 2, but has $T_\infty = 1200$ $^\circ$C, i.e. a cooler region at great depth. For an age of 10 My the temperature profile is still identical to the boundary layer cooling solution for a slow plate (top of figure) but departs slightly from the boundary layer cooling solution (dotted curve) for a fast plate (bottom of figure). At 150 My shear heating represents an important contribution to the heat balance and the temperature profile departs significantly from that of the simple boundary layer cooling case (dotted curve). This introduces a dependence of the thermal structure on the activation volume V^*. The temperature profiles for V^* between 11 and 30 $cm^3/mole$ lie in the shaded regions between the curves appropriate to these limiting values of V^*. Higher activation volumes imply higher temperatures for a given depth. Notice finally that the bump on the T-curve is more pronounced for the fast plate (bottom of Figure 3) than for the slow plate (top of Figure 3). At 150 My and $T_\infty = 1200$ $^\circ$C, the calculated surface heat flow is thus larger than the value 0.82 HFU for boundary layer cooling. Depending on V^* and plate velocity, q_o can be as large as 1.08 HFU (see Table 2).

We have thus seen that for certain plate ages and velocities, it is physically possible to have a steady state temperature vs. depth curve which exhibits a change in the sign of its curvature. This, in a one-dimensional model,

would only be possible if heat sinks were present, if the
thermal conductivity k had a peculiar T-dependence or,
of course, if the situation were not steady state. Here,
this phenomenon is related to the steady state advection
of colder material from below in the two-dimensional flow
field which will be described shortly.

The importance of shear heating in the oceanic asthen-
osphere is also illustrated by the fact that the functional
dependence of q_0 on $(T_\infty - T_0)$ is no longer the linear one
predicted by the simple boundary layer cooling solution
(see (15)). This is shown in Figure 4 where the calculated
value of q_0 at 1000 km from the ridge is shown vs. $(T_\infty - T_0)$
for plate velocities of 2, 5 and 10 cm/yr. The lower branches
of the curves refer to the non-Newtonian cases discussed so
far and the Newtonian I rheology (Table 1); the upper
branches are for the Newtonian II rheology (Table 1). Above
about 1400 $^\circ$C the linear relationship holds almost exactly,
i.e. viscous dissipation is negligible. For larger dis-
tances from the ridge we have seen that shear heating is
noticeable even for $T_\infty = 1600$ $^\circ$C (see q_0 in Table 2). Thus
the nonlinearity would be much more noticeable for older
ages than those of Figure 4.

Depth of the Decoupling Shear Zone

Horizontal velocity distributions $u(y)$ corresponding
to the above described temperature profiles for a dry
olivine mantle are also shown in Figures 2 and 3. The

associated viscosity profiles $\eta(y)$ are given in Figures 5 and 6, respectively; calculated values of the shear stress τ are listed in Table 3.

In Figures 2 and 3 we see that the horizontal velocity drops from its surface value of 2 or 10 cm/yr to zero in a narrow zone of shear, which we can also call the asthenosphere since it corresponds to a region where the viscosity reaches a minimum as seen in Figures 5 and 6. The rather strong rise in viscosity below the asthenosphere is related to the particular boundary condition we impose at great depth, i.e. $T = T_\infty$. For a finite heat flow from great depth, $q_\infty \neq 0$, the viscosity would rise less steeply below the asthenosphere.

The shear zone corresponding to a given geotherm is located in a depth range which depends upon the value of V^*, even when the geotherm is independent of V^*. For $V^* = 30$ cm^3/mole the reduction in horizontal velocity takes place at shallower depth than for $V^* = 11$ cm^3/mole. Since all solutions for intermediate values of V^* fall in between these two extreme velocity profiles, the included area has been shaded to indicate the range of possible solutions due to the uncertainty in the value of V^*. The observed upward shift of the shear zone when V^* increases, everything else being equal, simply indicates that when pressure effects in (25) or (27) become important, the system adjusts by moving up the shear zone. The depth of the shear zone is

a compromise between the opposing effects of temperature and
pressure which tend to move the shear zone downward and upward,
respectively. Thus in a given situation, the actual depth of
the asthenosphere is determined by the particular values of
the rheological parameters.

The width of the shear zone can be defined as the depth dif-
ference between u = 0.95 u_o and u = 0.05 u_o. From the figures we
see that the widths range from 60 to 150 km for an age of 10 My.

For a given value of the rheological parameter V*, the width
of the asthenosphere does not depend very strongly on the plate
velocity or age. This is apparent from the figures since the
respective u profiles are almost parallel to each other. One should
realize that the boundary condition q_∞ = 0 at great depth has an
influence on the location of the bottom of the shear zone. A nonzero
value of q_∞ is expected to extend the asthenosphere to greater depth.

The depth of the top of the shear zone, i.e. the plate
thickness, does not vary significantly with plate velocity,
as can be seen by comparing any pair of corresponding curves
u(y) for 2 and 10 cm/yr from the top and bottom parts of
Figures 2 or 3. The plate thickness, on the other hand,
exhibits a variation with age which will be analyzed in the
next section. Here we notice, by inspection of Figures 5
and 6, that the value of the viscosity in the asthenosphere,
i.e. in the shear zone, increases by up to one order of
magnitude as the plate age increases from 10 to 150 My. For
example, at a velocity of 2 cm/yr and V* = 30 cm^3/mole we
find, from Figures 5 and 6, that the viscosity minima for

$T_\infty = 1600$ $^{\circ}$C are 5.5×10^{19} and 2.0×10^{21} poises, for 10 and 150 My, respectively, and for $T_\infty = 1200$ $^{\circ}$C the viscosity minima are 1.2×10^{21} and 1.2×10^{22} poises for the two ages. This trend with age is less pronounced in cases where shear heating gives rise to strong departures of the old age geotherm from the simple boundary layer cooling solution. This is seen for the fast plate with $T_\infty = 1200$ $^{\circ}$C at the bottom of Figure 6.

The values of the shear stress τ obtained for the 16 cases discussed so far are listed in Table 3. The increase with age of the viscosity in the shear zone is seen to correspond to an increase of the shear stress with age. For instance, in the two examples just discussed, one sees that τ varies from 0.90 to 17.0 bars in the example of Figure 5 ($T_\infty = 1600$ $^{\circ}$C) and from 24 to 193 bars in the example of Figure 6 (1200 $^{\circ}$C), as age increases from 10 to 150 My. The latter value of τ is high and corresponds to a cold mantle ($T_\infty = 1200$ $^{\circ}$C) and an old (150 My), slow ($u_0 = 2$ cm/yr) plate with a stiff rheology ($V^* = 30$ cm^3/mole). Having this same plate move at 10 cm/yr generates more shear heating and τ drops to 75.5 bars. One notices the relatively lower magnitudes of the shear stresses for $T_\infty = 1600$ $^{\circ}$C as compared with $T_\infty = 1200$ $^{\circ}$C.

In situations where the entire heat production inside the model mantle is due to shear heating (Schubert and Turcotte, 1972; Froidevaux and Schubert, 1975) the shear stress τ is inversely proportional to the plate velocity

u_o if the heat flow is kept constant. Indeed, this heat
flow is equal to the energy dissipated τu_o in a steady
state regime. As heat is introduced by radioactive sources
or as in this paper, by advection, this simple behavior is
no longer true. Table 3 illustrates this point. An in-
crease of velocity by a factor 5, everything else being
equal, produces an increase in τ by a factor <2. When
strong viscous heating effects are present ($T_\infty = 1200\ ^\circ C$,
age of 150 My) the shear stress decreases by a factor 1.4
to 2.5. The assumption that τ is proportional to u_o, used
by various authors (Solomon and Sleep, 1974; Forsyth and
Uyeda, 1975; Solomon et al., 1975) in their discussions of
plate motion and of the possible driving forces, is thus not gener-
ally supported by thermo-mechanical models of plate de-
coupling.

Vertical Velocity Fields

The vertical velocity $v(y)$, taken as positive upward,
is also illustrated in Figures 5 and 6 for the 16 cases
based on a dry olivine rheology. For an age of 10 My, v
increases from zero just at the top of the asthenosphere
and approaches an asymptotic value of about 0.4 cm/yr in
the mantle below the asthenosphere. This is true both for
slow and fast moving plates. For 150 My the asymptotic
value of v drops below 0.1 cm/yr.

The upward-motion supplies the mass required for the accretion of the thickening plate. One may rationalize the fact that the asymptotic value of v is essentially dependent upon age, but independent of the plate velocity, by writing, from the continuity equation,

$$\int_0^Y dv = \frac{d}{dx} \int_0^Y u\, dy \tag{28}$$

or, because $x = (u_0 \cdot age)$ and $v_0 = 0$,

$$v_\infty = \frac{d}{d(age)} \int_0^\infty (\frac{u}{u_0})\, dy \tag{29}$$

For a given age, the u/u_0 profiles as plotted in Figures 2 or 3 are practically identical for slow and fast plates. Thus the above integral is nearly independent of plate velocity and so is v_∞. This result follows immediately if one assumes that the plate thickness is a function of age only. The next section will show that there are small departures from this approximation but that it is correct to within 20%. The spread in values of v_∞ for a given age is also about 20%.

A posteriori we may notice that the assumption v << u is valid within the boundary layer for ages larger than 10 My, but would not hold much nearer to the ridge axis. We recall also that shear heating due to $\frac{\partial v}{\partial x}$ was neglected in (18); a posteriori we see this term to be small compared to $\frac{\partial u}{\partial y}$.

Results for a Wet Olivine Mantle

Calculations based on the olivine rheology given in the second column of Table 1 have been carried out to determine the effects of the presence of water in the mantle on the thermal and mechanical structure of the oceanic lithosphere and asthenosphere. Figure 7 compares the solutions for a wet and dry olivine mantle, both with $V^* = 30$ cm^3/mole, $T_\infty = 1200$ °C and $u_0 = 10$ cm/yr. The simple boundary layer cooling profile (conduction) for an age of 150 My is shown for reference. The T and u profiles are only slightly different. The largest effect is at 150 My where the softer "wet" rheology reduces the amplitude of the viscous dissipation bump on the geotherm.

The smaller value of E^* in the wet olivine case yields values of the minimum viscosity η_{min} in the asthenosphere and values of the shear stress τ which are lower than those of corresponding dry olivine cases (see Table 4). Again we see that the drop in viscosity and shear stress is more marked at young age since at older ages shear heating can have some compensating feedback effect on the temperature. This feedback phenomenon was dominant in our study of the continental asthenosphere (Froidevaux and Schubert, 1975).

Solutions for a Newtonian Rheology

Six solutions for a Newtonian rheology with parameter values given in Table 1 are shown in Figures 8 (u and T) and

9 (η) for a fast plate (u_O = 10 cm/yr) and a cold lower
mantle (T_∞ = 1200 ^{O}C). The solid curves are for the New-
tonian I case with V* equal to either 11 or 30 cm^3/mole.
The same convention as in previous figures identifies a
particular value of V*. Recall that the shear zone is
shallower for larger V*. The shaded regions again denote
the range of solutions for intermediate values of V*, in
the Newtonian I case. The dashed curves are the solutions
for the Newtonian II set of parameter values.

The temperature, velocity and viscosity profiles can
first be compared with the results for a dry olivine mantle
shown at the bottoms of Figures 3 and 6, corresponding to
the same values of u_O and T_∞. The viscous heating bumps
--on the temperature profiles are much more marked in the
Newtonian cases and thus the depths of the shear zones
are rather shallower. The relatively higher temperatures
lead to values of the viscosity minimum between 10^{20} and
10^{21} poises for the Newtonian I parameters. These values
do not differ much from those of the corresponding dry
non-Newtonian cases. Furthermore, the shear stress values
are only a factor 1.5 to 2 larger than the corresponding
τ values for the dry non-Newtonian cases at 10 My and
become equivalent at 150 My (see Tables 3 and 5).

The comparison just discussed was between a rather
readily deformable Newtonian rheology (Froidevaux and
Schubert, 1975) and the relatively undeformable, dry
olivine nonlinear case. We have seen that in the

presence of water the non-Newtonian rheology is much "softer". Therefore, it may be more appropriate to compare the Newtonian I rheology with the wet olivine case, since both correspond to about the same value of the activation energy E^*. This comparison shows the non-Newtonian mechanism to be more efficient than the Newtonian I case, at least for the situation $T_\infty = 1200$ $^\circ$C and $u_0 = 10$ cm/yr.

The Newtonian II rheology leads to solutions with viscosities and shear stresses which are larger than those for the non-Newtonian cases, as can be seen in Figure 9 and Table 5. The Newtonian II set of rheological parameters therefore also describes a mechanism of deformation which is not competitive with the nonlinear olivine rheology. This remark applies again to a cold mantle ($T_\infty = 1200$ $^\circ$C) and a fast plate.

The Dominant Mechanism of Deformation

The Newtonian law of deformation for solids is based on atomic diffusion across grains under the influence of applied stress (Nabarro, 1948). In laboratory deformed olivine, this behavior has never been observed because the non-Newtonian process, based on the motion of dislocations (Weertman, 1970), is much more efficient. Naturally deformed peridotite nodules exhibit sub-grain structures and dislocation densities similar to those of samples deformed in the laboratory (Nicolas et al., 1973). Thus,

one might expect the non-Newtonian behavior to be dominant in the asthenosphere, wherein the peridotite nodules are believed to originate.

Our calculations can provide some insight to the question of what is the dominant mode of deformation in the mantle since we can compare values of shear stress for different sets of rheological parameters, other conditions being similar. However, there can be no definitive answer to this question since rheological parameter values for Newtonian deformation are purely speculative and we can only comment on the particular cases, Newtonian I and II, studied here.

Figure 10 shows the values of shear stress at 1000 km from the ridge crest for a fast plate (u_o = 10 cm/yr) and for four different sets of rheological parameters as functions of the postulated temperature increment between the surface and the mantle below the asthenosphere ($T_\infty - T_o$). The shear stress for wet olivine (curve b) is always smaller than τ for a dry olivine rheology (curve a). Similarly, the Newtonian I (curve d) shear stress is always smaller than that of the Newtonian II case (curve c).

The important comparison one would like to make, however, is between Newtonian and non-Newtonian cases for a dry or for a wet mantle. In the latter case, one compares curves d and b (if, in fact, the Newtonian I case represents the linear deformation of wet mantle rocks). For

$(T_\infty - T_O)$ less than 1350 ^{O}C the non-Newtonian rheology
yields smaller values of τ than the Newtonian I rheology;
for $(T_\infty - T_O) > 1350$ ^{O}C the situation is reversed. Thus,
at 1000 km from the ridge, i.e. for an age of 10 My, the
dislocation mechanism is dominant for a relatively cold
mantle, whereas for a relatively warm mantle the diffusion
mechanism is more efficient. One can thus conceive a
situation in which the deformation is essentially Newtonian
near the ridge, where we shall see that stress values are
small, and non-Newtonian under old oceans, where our cal-
culations show stress values to be larger.

We speculate that the Newtonian II rheology may be
appropriate to a dry mantle. It may also be the case that
the linear deformation of dry mantle rocks is even more
difficult than that of the Newtonian II case. Figure 10
shows that the dry non-Newtonian rheology yields values of
τ (curve a) smaller than those for the Newtonian II case
(curve c) for $(T_\infty - T_O) < 1600$ ^{O}C. Thus at 1000 km from
the ridge and for $u_O = 10$ cm/yr, the dislocation mechanism
would be more efficient if the mantle is dry.

The comparisons discussed above are illustrative of
those that must be made at all distances from the ridge as
a function of u_O and $(T_\infty - T_O)$. Different mechanisms of
deformation may be dominant in different locations rela-
tive to ridge and trench and for different plate velocities
and sub-asthenospheric temperatures. Non-Newtonian behavior
certainly prevails in regions of large stress, whereas

Newtonian deformation takes over in regions of low stress.
On Figure 10 the cross-over occurs around 1 bar. For
high enough temperatures at shallow depth, (19) can still
lead to important deformations even for low stress values.
The limitation on the present state of knowledge of the
rheological behavior of the mantle comes partly from the
fact that laboratory experiments cannot be performed at
low enough stress to measure the Newtonian parameters.

AGE DEPENDENCES OF THERMAL AND MECHANICAL

PROPERTIES OF THE LITHOSPHERE AND ASTHENOSPHERE

Lithosphere Thickness

In discussing the thickness of the lithosphere and how this thickness increases with age, one must first be precise about the definition of this quantity. Since the term lithosphere is generally understood to refer to the essentially rigid plates at the Earth's surface, a mechanical definition of lithosphere thickness seems appropriate. We define lithosphere thickness to be the depth at which $u/u_O = 0.95$; above this depth there is essentially no deformation, while below it there is a region of strong shear, the asthenosphere. Others, because of either the geophysical data they consider (seismic or heat flow) or limitations of the theoretical model they use to describe the lithosphere (the mechanical structure of the lithosphere has not heretofore been modelled) have employed the term lithospheric thickness to indicate the depth of a particular isotherm or a characteristic depth of a seismic wave velocity model.

Figure 11 shows the thickness of the rigid lithosphere, defined above, as a function of $(age)^{\frac{1}{2}}$ and age, for different rheologies, rheological parameter values, plate velocities, and for a deep temperature $T_\infty = 1200\ ^OC$. The solid curves

are for the dry non-Newtonian rheology; for the upper two
solid curves V* = 11 cm^3/mole and for the lower two solid
curves V* = 30 cm^3/mole. Plate velocity distinguishes
between the two solid curves for each value of V*; the
one with the larger thickness is for u_o = 2 cm/yr, the
other is for u_o = 10 cm/yr. The dashed curves are for
the Newtonian I rheology and u_o = 10 cm/yr; the upper
dashed curve is for V* = 11 cm^3/mole, the lower one is
for V* = 30 cm^3/mole. Finally, the long-short dashed
curve is for the Newtonian II rheology and u_o = 10 cm/yr.

The lithosphere is observed to thicken with age, but
it grows more slowly than (age)$^{1/2}$. As we noted earlier, the
lithosphere is thicker the smaller the activation volume
and the smaller the plate velocity, other quantities being
the same. In general, the rate of growth of the lithosphere
decreases with age, an effect which appears to be more pro-
nounced under conditions wherein viscous dissipation con-
tributes significantly to the thermo-mechanical structure
(thus, for T_∞ = 1600 $^\circ$C the effect would be less apparent).
For example, in the case of the dry non-Newtonian rheology
with V* = 30 cm^3/mole, T_∞ = 1200 $^\circ$C and u_o = 10 cm/yr, the
lithosphere thickness at an age of 10 My is 40 km. If
this lithosphere thickened with (age)$^{1/2}$ it would be about
155 km thick at 150 My; however, according to Figure 11 it
is only 100 km thick at 150 My. The thickening of the
lithosphere with age is mainly the result of boundary layer

cooling. Viscous heating, especially at older ages tends
to reduce the rate of growth of the boundary layer or
lithosphere.

Although, as discussed above, we cannot directly
compare our determinations of lithosphere thickness based
on the mechanical definition with that inferred from model
inversions of surface wave phase velocities (Leeds et al.,1974;
Forsyth, 1975; Leeds, 1975), a qualitative comparison may be worth
noting. Leeds (1975) concludes that the lithosphere con-
tinues to thicken even 100 My after formation, in agreement
with the results of our study. A quantitative comparison
of the rate of thickening is unwarranted in view of the
differences in definition of lithosphere thickness and
the dependence of the seismically inferred thickness on
the model used in the inversions. Another piece of
evidence for a continuous thickening of the oceanic
lithosphere may be the fact that old plates require a
longer time to be thermally equilibrated after they plunge
into the mantle at the trenches (Deffeyes, 1972).

Our results are to be contrasted with those of
McKenzie (1967) and Parsons and Sclater (1976) who assume,
a priori, a lithosphere of constant thickness and
Oldenburg (1975) who finds that the lithosphere thickens
proportionally with $(age)^{1/2}$.

Heat Flow

Figures 12 and 13 show the surface heat flux q_o in
HFU (1 $\mu cal/cm^2$-sec) as a function of age in My. Also
included in the figures are curves of shear stress as a
function of age; these will be discussed in a separate
sub-section. The heat flow curves show values of q_o
which decrease with age. Figure 12 presents the heat flow
for the non-Newtonian rheology; cases a and b are dry
olivine and wet olivine, respectively, with $v^* = 30$ cm^3/mole.
The curves in the upper part of the figure are for $u_o =$
2 cm/yr and those in the lower part have $u_o = 10$ cm/yr.
Heat flux results shown in Figure 13 are based on the
Newtonian rheologies, the solid curves for the Newtonian I
parameter values and the dashed curve for the Newtonian II
case. The numbers 30 and 11 labelling the solid curves
in Figure 13 refer to the values of activation volume in
cm^3/mole. The deep temperature T_∞ for the results of both
Figures 12 and 13 was again 1200 ^oC. Finally, the dotted
lines in the figures show the heat flow q_o as a function
of age for the simple boundary layer cooling situation,
wherein the surface heat flux decreases with the reciprocal
of (age)$^{\frac{1}{2}}$. The dotted lines therefore have slopes of $-\frac{1}{2}$.

The solutions of Figures 12 and 13, which include
thermo-mechanical coupling and viscous dissipation, show
noticeable departures from the inverse square root
dependence on age. The departure of q_o from the inverse

square root dependence on age becomes more pronounced
with increasing age; all the curves have an upward curva-
ture and show a tendency to flatten at old ages. There
is a difference between the q_o of the simple boundary layer
cooling solution and the solutions of Figures 12 and 13 even
at young ages. Particularly apparent is the excess heat
flux at 10 My and older associated with viscous dissipa-
tion in two of the Newtonian cases of Figure 13 and in the
non-Newtonian case of Figure 12, u_o = 10 cm/yr (curves a
and b in the lower part of Figure 12). For the slowly
moving plate (u_o = 2 cm/yr, upper part of Figure 12), shear
heating effects for the wet olivine rheology are noticeable
only after about 100 My, while the dry olivine rheology
leads to appreciable viscous dissipation beyond about 20 My.

The heat generated by viscous dissipation adds to
that of boundary layer cooling and tends to displace the
q_o curve upward from the straight line associated with
boundary layer cooling, and because shear heating becomes
more important with age, it tends to flatten the q_o curve
with increasing age. A comparison of the Newtonian curves in
Figure 13 shows that the larger V^*, the larger the contribution
of viscous dissipation to q_o and the greater the flattening
of the q_o vs. age curve at older ages, other quantities
being equal. Figure 12 shows that there is a modest increase
in q_o for higher values of plate velocity.

Sclater et al. (1976) have reconsidered the age dependence
of heat flow averages for the North Pacific. Their heat flow
averages included data only from sites with a thick layer of
"impermeable" sediment, since it is generally believed that hydro-
thermal circulation can transport a significant amount of heat
(Elder, 1965) whereas the measurements only reflect that portion
of the total heat being conducted through the sediments (Lister,
1972, 1974). Figure 14 compares these average heat flows, shown
by the shaded rectangles, with three theoretical surface heat
flux curves derived from our model. The vertical and horizontal
dimensions of each box are estimates of the uncertainties in
heat flow and age, respectively (Sclater et al., 1976). The
filled circles with associated error bars are data for the
North Pacific from Sclater and Francheteau (1970). The solid
curve is for a wet olivine rheology with an activation volume
of 11 $cm^3 mole^{-1}$ and T_∞ = 1600 $^O C$; the long and short dashed
curves are for V^* = 30 $cm^3 mole^{-1}$ and 11 $cm^3 mole^{-1}$, respectively,
with a dry olivine rheology and T_∞ = 1200 $^O C$. The plate velocity
in all three cases is 10 $cmyr^{-1}$, appropriate for the fast Pacific
plate.

The averages of Sclater et al. (1976) are consistent with
a heat flow proportional to $(age)^{-\frac{1}{2}}$ for most of the ocean floor
and suggest a flattening of the heat flow in the ocean floor
older than about 100 My. These heat flow averages are in quali-
tative agreement with the results of our model. With T_∞ = 1200 $^O C$,
viscous heating produces a flattening of the theoretical heat
flow curves for the older ocean floor. For T_∞ = 1600 $^O C$, shear

heating does not contribute significantly to the theoretical surface heat flux. One might argue that available heat flow values for old oceans could be used to determine what T_∞ or what rheological parameters are appropriate for the Earth. Figure 14 shows, however, that oceanic heat flow measurements are not yet accurate enough to discriminate among the various cases. In particular, we do not feel that T_∞ can presently be inferred by this method. Additional factors not considered in our present model, such as mantle radioactivity, further complicate the task of choosing preferred values of T_∞ or rheological parameters.

Shear Stress

The dependence of shear stress τ on age of the ocean floor is also shown in Figures 12 and 13; parameter values for the different curves follow the same convention as given previously for the heat flux values. Shear stress is seen, in general, to increase with age of the ocean floor; for the Newtonian II rheology, however, there is a slight decrease of τ with age (Figure 13). A larger activation volume implies a larger τ, other parameters being equal. The shear stress for dry olivine is larger than that of the wet olivine for the same value of V*.

The magnitude of τ lies between about 10 and 100 bars for the cases shown in Figures 12 and 13 ($T_\infty = 1200\ ^\circ C$). For very young ages, higher T_∞ values and for more readily deformable

rocks, e.g. a wet olivine with $V* = 11$ cm^3/mole, τ can be as small as a fraction of a bar to several bars. We have also seen in Figure 10 that higher sub-asthenospheric temperatures lead to lower values of shear stress. Solomon et al. (1975) have inferred shear stresses of a few bars at the base of oceanic plates from their studies of intraplate stresses.

One may integrate the shear stress vs. age relationships given in the figures to obtain the total drag force per unit length of ridge acting on a lithospheric plate. For both the Pacific and Atlantic plates the total drag force per unit length of ridge would be of the order of $10^{16}-10^{17}$ dynes/cm if conditions are such that the τ values of Figures 12 and 13 apply. If this had to be balanced by a pull from the downgoing slab at the trench, it would imply a downward force per unit depth and per unit length of trench of 1-10 kbars. This may be somewhat too high although Schubert et al. (1975) have found that the downward force on the slab due to thermal contraction and phase boundary elevation may be several kbars per unit length of trench and per unit depth. The drag force may be one to two orders of magnitude smaller, especially for higher values of T_∞. Froidevaux and Schubert (1975) found shear stresses beneath continents to be of the order of 200 bars for temperatures at 400 km comparable with T_∞ values considered here. The addition of radioactive heat sources in the continental mantle reduced the shear stress to 40 bars. It is thus fair to say, by comparison, that the stresses under oceanic plates are smaller by one order of magnitude or more. It is quite possible however that

different rheological properties prevail under the two
types of provinces. Our conclusion is in agreement with
that of Forsyth and Uyeda (1975) based on their study of
the relative forces acting on plates in dynamic equilibrium.
They found that the drag resisting plate motion
is stronger under the continents than under the oceans.
The type of data required to throw some light on this
problem is a detailed comparative study of the disloca-
tion structure and density in the sheared peridotite
nodules from oceanic and continental origin.

We have noted earlier that $d\tau/dx$ must be small com-
pared with ρg if the mathematical formulation of our
model is valid. From Figures 12 and 13 one finds that
$-d\tau/dx$ is at most about 0.5 dynes/cm^3 and is usually sig-
nificantly less, whereas ρg is about 3×10^3 dynes/cm^3.
Thus our approximation $d\tau/dx \ll \rho g$ is an excellent one;
it says that the pressure is purely lithostatic.

The net state of stress in the lithosphere is a
complex superposition of thermal and mechanical stresses
obviously not accounted for by our model. This precludes
a direct comparison of intraplate stresses inferred from
earthquake source mechanisms with the τ values computed
here. Since intraplate stresses inferred from earthquake
source mechanisms and in-situ measurements reflect the
resultant, in the elastic part of the lithosphere, of
various large scale forces acting at plate boundaries
(Sbar and Sykes, 1973) and of more local stresses, they

cannot directly compare with the shear stress values of
our model. Our shear stress values, represent the viscous
drag acting beneath the plates.

Bathymetry

As discussed in the section on the mathematical
formulation of our model, the thermal contraction and densi-
fication of the lithosphere as it moves away from the ridge
and cools, can be interpreted as giving rise to the topography
of the ocean floor via the mechanism of isostatic compensa-
tion. Using equation (4), we have calculated the depth of
the ocean floor as a function of age for the dry non-
Newtonian case with $T_\infty = 1200\ ^\circ C$, $u_o = 10$ cm/yr and $V* =$
_11 and 30 cm^3/mole. The results are shown in Figure 15
where the depth of the ocean is plotted as a function of
$(age)^{\frac{1}{2}}$; the upper part of the figure is for an expansion
coefficient $\alpha = 3 \times 10^{-5}\ K^{-1}$ and the lower part is for $\alpha =$
$4 \times 10^{-5}\ K^{-1}$. The shaded region again represents the range
of topographic solutions for intermediate values of V*.
The figure also includes the topography associated with
the simple boundary layer cooling solution computed on
the basis of (16) (the dashed curves). Finally, bathyme-
tric data for the Pacific ocean, taken from the summary of
Parsons and Sclater (1976), are shown on the figure (open
circles are based on depths from topographic profiles,
closed circles are based on depths from Joides sites).

Since depth increases as $(age)^{\frac{1}{2}}$ in the simple boundary
cooling solution (equation (16)), the slopes of the straight

dashed lines indicate this functional dependence. Note that the slope depends on α and thus is different in the upper and lower parts of the figure. It is clear that the data depart from the straight line for ages greater than 80-100 My. The ocean floor beyond 100 My is not as deep as would be predicted by simple boundary layer cooling. It is also obvious in the figure that <u>our thermo-mechanical model of the oceanic lithosphere and asthenosphere yields depths which depart significantly from the (age)$^{\frac{1}{2}}$ law, showing considerable flattening as a function of age.</u> In the upper part of the figure, for $\alpha = 3\text{x}10^{-5}$ K^{-1}, it is seen that no reasonable value of V* would yield topography in good agreement with the data while in the lower part of the figure, for $\alpha = 4\text{x}10^{-5}$ K^{-1}, one can see that a V* somewhat larger than 11 cm^3/mole would adequately match the observations. These statements are true for the boundary condition $T_\infty = 1200$ ^{O}C. For higher values of T_∞ shear heating effects are less pronounced and a higher V* value and/or a smaller α value are more appropriate to fit the data. Such trade-offs of parameters are often characteristic of geophysical modelling.

The flattening of ocean floor topography with age is a consequence of the viscous dissipation in our model. Frictional heating in the shear zone that constitutes the asthenosphere offsets the conductive cooling of the lithosphere as it moves away from the ridge. The shear heating tends to maintain the material at a higher temperature as a function of age than if the material were simply cooling by conduction. Thus less thermal contraction occurs and the lithosphere remains lighter with age;

the depth of the ocean floor therefore need not increase
as rapidly as $(age)^{\frac{1}{2}}$ to maintain a state of isostatic compensation.

The model of Parsons and Sclater (1976) also shows an
ocean floor topography that tends to flatten with age.
However, their result is a consequence of an a-priori specified feature of their model, namely that the lithosphere
is of constant thickness for all ages. There is no physical mechanism in their model, such as the shear heating
in ours, which is responsible for the flattening of the
topography. We recall that our results, discussed at the
beginning of this section, show that the lithosphere continues to increase in thickness even at old ages.

Seismic Velocities

Our model is that of a pure olivine mantle. This
approximation is justified by the fact that olivine is
the main constituent of the upper mantle, and that observations of peridotite nodules (Nicolas et al., 1973) show
that olivine is more abundant and deforms more readily than
the pyroxenes and other minerals contained therein. However, an investigation of the elastic properties of the
oceanic mantle certainly requires a more adequate petrological model and the inclusion of possible phase changes. In
particular, it should be decided whether or not the asthenosphere is a zone of partial melting. Our model does not
require partial melting for a zone of mechanical decoupling, since solid state deformation yields sufficiently low

viscosities. On the other hand, it is known from the
study of metallic phases (Auten and Gordon, 1975) that a
small amount of partial melting does not substantially
alter the subsolidus deformation law, since the grains
must still be deformed in their bulk to allow shear on a
large scale. This is also true for rocks (Arzi, 1972).
Hence, we have not, till now, been concerned with whether
the computed geotherms cross the solidus of mantle material.

Figure 16, representing seismic velocities vs. depth
for ages of 10 My and 150 My, has been drawn on the basis
of elastic parameters for pure dry olivine (Kumazawa and
Anderson, 1969). The solid lines with the most pronounced
velocity minima are for $T_\infty = 1600\ ^\circ C$, the other solid
lines are for $T_\infty = 1200\ ^\circ C$ and the area in between is
shaded; both cases are for a slow plate ($u_0 = 2$ cm/yr).
The dashed solutions are for $u_0 = 10$ cm/yr, $T_\infty = 1200\ ^\circ C$
and $V^* = 30$ cm^3/mole, i.e. for a geotherm exhibiting a well
developed shear heating bump. At 10 My this case falls on
the solid line for $T_\infty = 1200\ ^\circ C$. For their prefered con-
tinental geotherm under old shields, Froidevaux and Schubert
(1975) obtained a flat seismic velocity profile in the
asthenosphere. Here, on the contrary, a marked minimum
develops around 50 km depth for an age of 10 My and below
100 km depth for an age of 150 My. This contrast between
oceanic and continental upper mantle seismic velocity pro-
files is in good agreement with seismological evidence
(Knopoff, 1972; Press, 1972; Jordan, 1975). Furthermore,the amplitud

of this seismic velocity drop, as seen from Figure 16, is

of the right magnitude, between 0.2 and 0.45 km/sec, for

shear waves. The presence of a molten phase would of

course amplify these drops, perhaps by an embarrassingly

large amount.

Studies of Rayleigh waves (Leeds, 1975) are usually

analyzed by assuming a constant value of v_s in the top part

of the upper mantle, the seismologist's lithosphere, and a

value 0.5 km/sec lower in the low velocity channel, the

seismologist's asthenosphere. Our model suggests that the

velocity drop, obtained on the basis of pressure and tem-

perature effects alone for an unsophisticated petrology, is

smaller for older ages, as can be seen in Figure 16. This

conclusion would still be qualitatively correct if partial

melting occurred in the shear zone. The flattening of

the geotherm with age implies that partial melting would

be more pronounced, or restricted, to young ages. For

example, Figure 17 shows that the temperature profiles

of the purely thermal solutions of (7) for $T_\infty = 1200$ $^\circ$C

do not intersect the solidus curve for a dry mantle

(curve a). In the presence of

hydrated minerals (curve b) this conclusion still holds.

For higher values of T_∞ the temperature of the solidus is

exceeded, in particular for young ages. Curve 'c' in Figure 17

is the solidus for a completely wet mantle. The solid lines

a, b and c are from Kushiro et al. (1968). The dashed

solidus is that given by Ito and Kennedy (1967) for dry

peridotite.

These remarks are not applicable to the region of
the ridge crest, since our model is for ages larger than
10 My. At the ridge crest, the high attenuation of
seismic waves testifies to the presence of a fraction of
melt (Solomon, 1973), also required to generate the
tholeitic basalts forming the new oceanic crust. What
is strongly needed is a series of seismological experi-
ments parallel to the ridge axis with ocean-bottom seis-
mometers. This should help to settle the problem of the
extent of partial melting in the oceanic asthenosphere.

The low velocity channel corresponding to strong
temperature gradients in the oceanic lithosphere does
not coincide, in depth, with the shear zone. This can
be seen by comparing the depths of the seismic velocity
minima in Figure 16 with the depths of the viscosity minima
in Figures 3 or 6. The seismologist's low velocity zone
is thus probably shallower than the asthenosphere defined
as the zone of decoupling of the plate from the mantle
below.

CONCLUDING REMARKS

Previous models of the oceanic lithosphere have all
been purely thermal, i.e. the velocity fields are not
derivable therefrom in a self-consistent manner owing to the
coupling of thermal and mechanical fields via the depend-
ence of viscosity on temperature and via viscous dissipation.
The main emphasis in this paper has been on the development
of a coupled thermomechanical subsolidus model of the oceanic
lithosphere and asthenosphere and on the exploration of the
consequences thereof. For example, what departures from
the simple $(age)^{\frac{1}{2}}$ dependences for such observables as ocean
floor depth result from thermomechanical coupling? Also,
what are the velocity profiles beneath the oceans and what
are the mechanical lithosphere and asthenosphere thicknesses
derived therefrom?

We have found that simple boundary layer cooling with
its direct and inverse proportionalities of ocean bottom
depth and ocean floor heat flux on $(age)^{\frac{1}{2}}$ is predominant at
young ages (not too near the ridge however). At older ages,
effects of viscous dissipation become more important, since
lithospheric cooling and thickening tends to place the
asthenosphere at greater depths where the pressure-dependence
of the viscosity leads to higher values of viscosity in the
asthenosphere. Shear heating causes the ocean to deepen
less rapidly than $(age)^{\frac{1}{2}}$, the lithosphere to thicken more
slowly than $(age)^{\frac{1}{2}}$, and the surface heat flow to decrease

less rapidly than (age)$^{-\frac{1}{2}}$. The magnitudes of the shear
heating effects depend not only on age, but also on the
plate velocity and the activation volume of the deforma-
tion process.

Shear stresses and values of the minimum viscosity
in the asthenosphere generally increase as the age of the
ocean floor and are substantially smaller under the oceans
than under the continents, again mainly because of the
greater depth of the continental asthenosphere coupled
with the pressure-dependence of the viscosity. It is im-
portant to remember that the depth of the asthenosphere is
not imposed a priori but is calculated. Thus the drag
forces beneath plates with continents are larger than
those beneath oceanic plates.

Because of our emphasis on studying the physical
effects of thermomechanical coupling on lithosphere and
asthenosphere structure, we have not attempted to adjust
unknown parameters such as V* and T$_\infty$ to obtain the best
quantitative fit of our model results with observations of
such quantities   as heat flux and topography. Nor
have we tried to distinguish which of the rheological laws
provide the best fit to such data. Our qualitative com-
parisons with data leave no doubt that parameters can be
adjusted to have physically reasonable values which pro-
vide good quantitative fits to heat flow and topographic
data, for example. In fact, with V*, T$_\infty$ and the rheological
law to vary, in addition to other parameters (e.g. α in

the case of ocean floor topography), it is probably true that
many different combinations of parameter values will pro-
vide adequate fits to data.

More importantly, a number of physical effects not in-
cluded in our present study should be investigated before
attempting to quantitatively fit observations. For example,
the influences of radioactive heat sources in the oceanic
upper mantle and crust and a nonzero heat flow from great
depth need to be determined. We have already seen in our
study of the continental asthenosphere that the addition
of radioactivity could significantly reduce the shear
stress.

We need also to investigate the effects of a possible
shallow return flow in the asthenosphere forced by a non-
zero adverse pressure gradient. The approach of the pre-
sent paper can readily be modified to include this effect
thereby extending the work of Schubert and Turcotte (1972).
In particular, it is important to determine if a shallow return flow
is compatible with gravimetric and bathymetric data on the
basis of the more complete approach developed here. As
regards shear heating effects and associated departures
from (age)$^{\frac{1}{2}}$ laws it is clear that they are more important
in the return flow case.

Our present study of the oceanic lithosphere and
asthenosphere, like our previous investigation of the

continental asthenosphere, emphasizes the importance to
geodynamic modelling of acquiring more laboratory data
on the thermal and mechanical properties of minerals pre-
sent in the mantle. Particularly important in this connec-
tion are determinations of the activation volume for olivine.
In terms of field measurements, seismic observations which
yield velocity profiles and attenuation data as a function
of ocean floor age are vital for further progress in our
understanding of the structure of the oceanic lithosphere
and asthenosphere. It is equally hoped that studies of
phase equilibria and deformation patterns in peridotite
nodules found in kimberlites (Africa, Siberia) and in
basaltic lava flows (volcanic islands and continents) will
soon provide more constraints on the temperature and vel-
ocity profiles, as well as on the magnitudes of shear stress.
A major question which such observations could help answer
is the extent to which the asthenosphere may be partially
melted away from the ridge.

ACKNOWLEDGMENT

REFERENCES

Anderson, D. L. and C. Sammis, Partial melting in the upper
mantle, Phys. of Earth and Planet. Interiors, 3, 41-50,
1970.

Arzi, A. A., Experimental study of partial melting in natural
rocks and subsequent creep under low stress, Trans. Am.
Geophys. Union, 53, 513, 1972.

Auten, T. A. and R. B. Gordon, Compressive creep rate of par-
tially melted AlGa alloys, Metall. Trans., 6A, 584-586.
1975.

Clark, S. P., Jr., editor, Handbook of Physical Constants,
Geological Society of America, Memoir 97, p. 92, 1966.

Davis, E. E. and C. R. B. Lister, Fundamentals of ridge
crest topography, Earth Planet. Sci. Lett., 21, 405-
413, 1974.

Deffeyes, K. S., Plume convection with upper mantle temper-
ature inversion, Nature, 240, 539-544, 1972.

Elder, J. W., Physical processes in geothermal areas, in
Terrestrial Heat Flow, edited by W. H. K. Lee, pp. 211-
239, American Geophysical Union, Washington, D. C., 1965.

Elsasser, W. M., Convection and stress propagation in the
upper mantle, in The Application of Modern Physics
to the Earth and Planetary Interiors, edited by S. K.
Runcorn, pp. 223-246, Wiley-Interscience, New York,
1969.

Forsyth, D., The early structural evolution and anisotropy of the oceanic upper mantle, Geophys. J. Roy. Astron. Soc., 43, 103-162, 1975.

Forsyth, D. and S. Uyeda, On the relative importance of the driving forces of plate motion, Geophys. J. Roy. Astron. Soc., 43, 163-200, 1975.

Froidevaux, C. and G. Schubert, Plate motion and structure of the continental asthenosphere: A realistic model of the upper mantle, J. Geophys. Res., 80, 2553-2564, 1975.

Gueguen, Y. and J. M. Mercier, High attenuation and low velocity zone, Phys. Earth and Planet. Interiors, 7, 239, 1972.

Ito, K. and G. C. Kennedy, Melting and phase relations in a natural peridotite to 40 kilobars, Am. J. Sci., 265, 519-538, 1967.

Jordan, T. H., The continental tectosphere, Rev. Geophys. Space Phys., 13, 1-12, 1975.

Kausel, E. G., A. R. Leeds and L. Knopoff, Variations of Rayleigh wave phase velocities across the Pacific ocean, Science, 186, 139-141, 1974.

Knopoff, L., Observation and inversion of surface wave dispersion, Tectonophysics, 13, 497-519, 1972.

Kohlstedt, D. L. and C. Goetze, Low-stress and high temperature creep in olivine single crystals, J. Geophys. Res., 79, 2045-2051, 1974.

Kohlstedt, D. L., C. Goetze and W. B. Durham, Experimental deformation of single crystal olivine with applica-

tion to flow in the mantle, in Petrophysics: The

Physics and Chemistry of Minerals and Rocks, ed.

S. K. Runcorn, John Wiley & Sons, Ltd., London, 1976.

Kumazawa, M. and O. L. Anderson, Elastic moduli, pressure

derivatives and temperature derivatives of single

crystal olivine and single crystal forsterite, J.

Geophys. Res., 75, 5961-5972, 1969.

Kushiro, I., Y. Syono and S. Akimoto, Melting of a peridotite

nodule at high pressures and high water pressures,

J. Geophys. Res., 73, 6023-6029, 1968.

Langseth, M. G., Jr., X. LePichon and M. Ewing, Crustal

structure of mid-ocean ridges, 5. Heat flow through

the Atlantic ocean floor and convection currents,

J. Geophys. Res., 71, 5321-5355, 1966.

Leeds, A. R., Lithospheric thickness in the western Pacific,

Phys. Earth Planet. Interior, 11, 61-64, 1975.

Leeds, A. R., L. Knopoff and E. G. Kausel, Variations of

upper mantle structure under the Pacific ocean,

Science, 186, 141-143, 1974.

Lister, C. R. B., On the thermal balance of a mid-ocean ridge,

Geophys. J. Roy. Astr. Soc., 26, 515-535, 1972.

Lister, C. R. B., On the penetration of water into hot

rock, Geophys. J. Roy. Astr. Soc., 39, 465-509, 1974.

McKenzie, D. P., Some remarks on heat flow and gravity anom-

alies, J. Geophys. Res., 72, 6261-6273, 1967.

Nabarro, F. R. N., Deformation of crystals by the motion of

single ions, in Conference on the Strength of Solids,

pp. 75-90, Physical Society, London, 1948.

Nicolas, H., F. Boudier and A. M. Boullier, Mechanisms of
flow in naturally and experimentally deformed peridotites,
Am. J. Sci., 273, 853-876, 1973.

Oldenburg, D. W., A physical model for the creation of the
lithosphere, Geophys. J. Roy. Astr. Soc., 43, 426-451,
1975.

Parker, R. L. and D. W. Oldenburg, Thermal model of ocean
ridges, Nature, 242, 137-139, 1973.

Parsons, B. and J. G. Sclater, An analysis of the variation
of ocean floor heat flow and bathymetry with age, sub-
mitted to J. Geophys. Res., 1976.

Post, R. L., The flow laws of Mount Burnett dunite, Ph.D.
thesis, Univ. of Calif., Los Angeles, 1973.

Press, F., The earth's interior as inferred from a family of
of models, in The Nature of the Solid Earth, edited by
E. C. Robertson, pp. 147-171, McGraw-Hill, New York,
1972.

Sbar, M. L. and L. R. Sykes, Contemporary compressive stress
and seismicity in Eastern North America; an example of
intraplate tectonics, Bull. Geol. Soc. Am., 84,
1861-1882, 1973.

Schatz, J. F. and G. Simmons, Thermal conductivity of earth
materials at high temperatures, J. Geophys. Res., 77,
6966-6983, 1972.

Schubert, G. and D. L. Turcotte, One-dimensional model of
shallow mantle convection, J. Geophys. Res., 77, 945-

951, 1972.

Schubert, G., D. A. Yuen, and D. L. Turcotte, Role of phase
transitions in a dynamic mantle, Geophys. J. Roy. Astron.
Soc., 42, 705-735, 1975.

Sclater, J. G. and J. Francheteau, The implication of ter-
restrial heat flow observations on current tectonic and
geochemical models of the crust and upper mantle of the
earth, Geophys. J. Roy. Astro. Soc., 20, 509-537, 1970.

Sclater, J. G., J. Crowe and R. N. Anderson, On the reliability
of oceanic heat flow averages, J. Geophys. Res., in press,
1976.

Solomon, S. C., Shear wave attenuation and melting beneath the
mid-Atlantic ridge, J. Geophys. Res., 78, 6044-6059, 1973.

Solomon, S. C. and N. H. Sleep, Some simple physical models for
absolute plate motion, J. Geophys. Res., 79, 2557-2567, 1974.

Solomon, S. C., N. H. Sleep and R. M. Richardson, On the forces
driving plate tectonics: Inferences from absolute plate
velocities and intraplate stress, Geophys. J. Roy. Astr.
Soc., in press, 1975.

Turcotte, D. L. and E. R. Oxburgh, Finite amplitude convective
cells and continental drift, J. Fluid Mech., 28, 29-42, 1967.

Turcotte, D. L. and E. R. Oxburgh, Mantle convection and the
new global tectonics, Ann. Rev. Fluid Mech., 4, 33-68,
1972.

Weertman, J., The creep strength of the earth's mantle, Rev.
Geophys. Space Phys., 8, 145-168, 1970.

DRY NON-NEWTONIAN (OLIVINE)	WET NON-NEWTONIAN (OLIVINE)	NEWTONIAN I	NEWTONIAN II
$n = 3$	$n = 3$	$n = 1$	$n = 1$
$E^* = 125 \frac{kcal}{mole}$	$E^* = 93 \frac{kcal}{mole}$	$E^* = 95 \frac{kcal}{mole}$	$E^* = 104 \frac{kcal}{mole}$
$V^* = 11\text{-}30 \frac{cm^3}{mole}$	$V^* = 11\text{-}30 \frac{cm^3}{mole}$	$V^* = 11\text{-}30 \frac{cm^3}{mole}$	$V^* = 9 \frac{cm^3}{mole}$
$B_3 = 6.45 \times 10^{-13} \frac{cm^3 sec^5 K}{gm^3}$	$B_3 = 5.41 \times 10^{-15} \frac{cm^3 sec^5 K}{gm^3}$	$B_1 = 2.4 \times 10^{-3} \frac{cmsecK}{gm}$	$B_1 = 1.81 \times 10^{-4} \frac{cmsecK}{gm}$
Kohlstedt and Goetze (1974) and Kohlstedt et al. (1975)	Post (1973)	Froidevaux and Schubert (1975)	Schubert and Turcotte (1972)

Table 1. Rheological Parameter Values

u_o (cm/yr) \ $V^* \left(\frac{cm^3}{mole}\right)$, T AGE	1200 °C		1600 °C	
	11	30	11	30
2 / 10 My	3.16*	3.16*	4.23*	4.23*
10 / 10 My	3.17	3.23	4.23*	4.23*
2 / 150 My	0.82*	0.93	1.09*	1.09*
10 / 150 My	0.88	1.08	1.09*	1.13

Table 2. Surface heat flow values q_o for a dry non-Newtonian rheology. Here q_o is defined positive upward and is given in HFU ($\mu cal/cm^2$ sec). The asterisk denotes that the value is identical to that of simple boundary layer cooling.

u_o (cm/yr)	AGE	$V^* (\frac{cm^3}{mole})$ 1200 °C		1600 °C	
		11	30	11	30
2	10 My	7.2	24.0	0.31	0.90
10		11.8	34.0	0.53	1.53
2	150 My	36.0	193	1.03	17.0
10		25.8	75.5	1.71	19.3

Table 3. Shear stress values (bars) for the dry non-Newtonian solutions.

RHEOLOGY / AGE		DRY OLIVINE	WET OLIVINE
10 My	Value of	3.1×10^{20}	6.5×10^{19}
150 My	η_{min} (poises)	7.7×10^{20}	6.8×10^{20}
10 My	Value of	34	6.2
150 My	τ (bars)	75	44

Table 4. Comparison of viscosity minimum η_{min} and shear stress τ values for wet and dry olivine rheologies with $T_\infty = 1200°C$, $u_0 = 10$ cm/yr and $V* = 30$ cm^3/mole.

RHEOLOGY AGE	NEWTONIAN I $V*=11$ cm^3/mole	NEWTONIAN I $V*=30$ cm^3/mole	NEWTONIAN II
10 My	14.5	109	187
150 My	46.2	126	91.4

Table 5. Values of shear stress (bars) for the Newtonian solutions
($T_\infty=1200^\circ C$, $u_o=10$ cm/yr).

FIGURE CAPTIONS

Figure 1.   Sketch of the model showing the thickening

oceanic lithosphere and the asthenosphere be-

neath. The left hand side of the diagram lists

the quantities that are inputs to the model;

the right hand side of the figure shows those

quantities which are outputs from the calcula-

tions. Note the two-dimensional flow in the

asthenosphere; the vertical motion supplies the

material to the growing lithosphere. T is temper-

ature, u, v are horizontal and vertical veloci-

ties, τ is shear stress. There are no sharp

boundaries to the asthenosphere. The boundaries

shown here have artistic value only.

Figure 2.   Temperature T and horizontal velocity u pro-

files for a dry olivine rheology as defined in

Table 1, column 1, $T_\infty = 1600$ $^\circ$C and $u_o = 2$ and

10 cm/yr for the top and bottom parts, respec-

tively. Solutions are plotted for two extreme

values of V*, 11 and 30 cm^3/mole, and for two

ages, 10 and 150 My. Temperature profiles are

insensitive, at the accuracy of our graph, to

the value of V*. This is not so for the velocity

curves. For a given age and u_o the lower u vs.

depth curve always corresponds to V* = 11 cm^3/mole,

the upper one to V* = 30 cm^3/mole. The shaded

area between two such curves represents the
range of solutions for intermediate values of
V*. The T profiles obtained for the simple
boundary layer cooling problem are identical
with the two profiles seen at the top of this
figure. For u_0 = 10 cm/yr and an age of 150 My
the above T vs. depth curve differs significantly
from the boundary layer cooling solution.

Figure 3. Temperature T and horizontal velocity u pro-
files for a dry olivine rheology. The format
is identical to that of Figure 2. Here T_∞ =
1200 $^\circ$C. For an age of 150 My the temperature
profiles are now split. The upper curve is
for V* = 30 cm^3/mole, and the lower one is for
V* = 11 cm^3/mole. The splitting of the u pro-
files is as in Figure 2 and the shading again
indicates the range of solutions for intermedi-
ate V* values. The dotted curves represent
the temperature profiles for simple boundary
layer cooling with variable thermal conductivity.
In the top part (slow plate) these solutions
are practically identical to the 10 My and
150 My, V* = 11 cm^3/mole, curves, respectively.

Figure 4. Surface heat flow vs. the temperature differ-
ence between the deep mantle and the surface
$(T_\infty - T_0)$ at a distance of 1000 km from the
ridge and for plate velocities of 10, 5 and 2
cm/yr. For a given plate velocity, the lower

branch is for both non-Newtonian rheologies
of Table 1 as well as for the Newtonian I
rheology and the upper branch is for the New-
tonian II rheology. These results are for
$V^*=11$ cm^3/mole, except of course for the
Newtonian II case.

Figure 5. Effective viscosity $\eta(27)$ and vertical velocity v
profiles for a dry olivine rheology and for the same
T_∞, u_0, V^* and age values as in Figure 2. The
top part of the figure is for u_0 = 2 cm/yr and
the lower part is for u_0 = .10 cm/yr. Vertical
velocity is positive upward. For a given age,
e.g. 10 My or 150 My, there are two solutions,
one for V^* = 11 cm^3/mole, the other for V^* =
30 cm^3/mole, specifically indicated for the
10 My case at the top of the figure. For the
other sets of solutions, the respective posi-
tions of the 11 and 30 cm^3/mole curves are simi-
lar. The shaded areas only approximately
represent the range of solutions for intermedi-
ate V^* values since solution curves for differ-
ent V^* values intersect.

Figure 6. Effective viscosity $\eta(27)$ and vertical velocity v
profiles for a dry olivine rheology with $T_\infty=1200$ $^\circ C$
and u_0 = 2 cm/yr (top) or 10 cm/yr (bottom).
Vertical velocity is positive upward. The
format is similar to that of Figure 5 and the
solutions are the η and v profiles corresponding

to the T and u profiles of Figure 3. The shaded
regions suggest the range of solutions for values
of V* between 11 and 30 cm^3/mole.

Figure 7. Comparison of temperature T and horizontal
velocity u profiles for wet and dry olivine
rheologies for ages of 10 and 150 My and for
T_∞ = 1200 ^{o}C, u_o = 10 cm/yr, V* = 30 cm^3/mole.
The temperature profile at 150 My for simple
boundary layer cooling is also shown for refer-
ence (dotted curve). The dotted curve for
10 My is practically identical to the temper-
ature profile for the wet olivine case (solid
curve at 10 My).

Figure 8. Temperature T and horizontal velocity u profiles
for a Newtonian rheology with parameter values
given in Table 1, T_∞ = 1200 ^{o}C and u_o = 10 cm/yr.
The numbers on the figure indicate ages of 10 My
and 150 My. For each age 3 solutions are shown.
Solid lines correspond to the Newtonian I case
and two values of V*. The lower T and u pro-
files are for V* = 11 cm^3/mole, the upper ones
for V* = 30 cm^3/mole. The shaded area between
these curves indicates the range of solutions
for intermediate values of V*. The dashed
lines are solutions for the Newtonian II case.

Figure 9. Viscosity profiles for a Newtonian rheology.
Three solutions are shown for each of the ages
10 My and 150 My. They correspond to the cases
illustrated in Figure 8. For the Newtonian I
rheology (solid lines) and a particular age,
the curve with the lower minimum viscosity
corresponds to $V* = 11$ cm^3/mole, the other one
to $V* = 30$ cm^3/mole. Again the area between
these two curves is indicative of solutions for
intermediate $V*$ values. The dashed curves are
the viscosity profiles for the Newtonian II
rheology. The inflection of the 10 My curve
below the region of minimum viscosity is due
to the large shear heating bump on the geotherm
for that case. Remember however that the rapid
increase of η below the asthenosphere is arti-
ficially imposed by the particular boundary
condition we choose for great depth, i.e. $T = T_\infty$.

Figure 10. Shear stress as a function of sub-asthenospheric
temperature $(T_\infty - T_o)$ for different sets of
rheological parameter values and $u_o = 10$ cm/yr,
$x = 1000$ km. a – dry olivine, $V* = 11$ cm^3/mole;
b – wet olivine, $V* = 11$ cm^3/mole; c – Newtonian
II; d – Newtonian I, $V* = 11$ cm^3/mole.

Figure 11.   Lithospheric thickness (depth at which u/u_o =

0.95) as a function of $(age)^{\frac{1}{2}}$. Solid curves -

dry non-Newtonian, dashed curves - Newtonian I,

long-short dashed curve - Newtonian II. The

Newtonian curves are for u_o = 10 cm/yr. The

upper dashed curve has V* = 11 cm^3/mole, the

lower dashed curve has V* = 30 cm^3/mole. For

the upper two solid curves V* = 11 cm^3/mole,

and for the lower two solid curves V* = 30

cm^3/mole. The value of u_o distinguishes the

solid curves with the same value of V*; the

thicker lithosphere is for u_o = 2 cm/yr,

the thinner one is for u_o = 10 cm/yr.

Figure 12.   Surface heat flow and shear stress as functions

of age. Heat flow decreases while shear stress increases

with age. Results are for non-Newtonian rheolo-

gy, V* = 30 cm^3/mole and T_∞ = 1200 ^oC. a - dry

olivine; b - wet olivine. The curves in the

upper part of the figure are for u_o = 2 cm/yr,

those in the lower part are for u_o = 10 cm/yr.

The dotted line is the surface heat flow vs.

age for simple boundary layer cooling. It is

a straight line with slope $-\frac{1}{2}$.

Figure 13.   Surface heat flux and shear stress as functions

of age. T_∞ = 1200 ^oC, solid curves - Newtonian I,

dashed curves - Newtonian II. 30 and 11 are values of V* in cm^3/mole. The dotted straight line is the simple boundary layer cooling, surface heat flow vs. age dependence; its slope is $-\frac{1}{2}$.

Figure 14. Heat flow at the ocean floor as a function of age for a wet olivine rheology with $T_\infty = 1600\ ^oC$ and V*=11 cm^3/mole (solid line), and for a dry olivine rheology with $T_\infty = 1200\ ^oC$ and V*=30 cm^3/mole (long-dashed line) and V*=11 cm^3/mole (short-dashed line). In all cases the plate velocity is 10 cm/yr. Heat flow data are from Sclater et al. (1976) (shaded rectangles) and Sclater and Francheteau (1970) (filled circles).

Figure 15. Bathymetry of the ocean floor as a function of $(age)^{\frac{1}{2}}$ for a dry olivine rheology with $T_\infty = 1200\ ^oC$, $u_o = 10$ cm/yr and V* = 11 and 30 cm^3/mole. The shaded regions represent the bathymetry solutions for intermediate values of V*. In the upper and lower parts of the figure α is $3 \times 10^{-5}\ K^{-1}$ and $4 \times 10^{-5}\ K^{-1}$, respectively. The dashed lines are the ocean floor depths for simple boundary layer cooling. The data points are from Parsons and Sclater (1975).

Figure 16. Seismic velocities (v_s - shear, v_p - compressional) vs. depth for 10 My and 150 My ages. For a

given age, the profile with the lower minimum

value of velocity is for $T_\infty = 1600$ ^{O}C, while

the other is for $T_\infty = 1200$ ^{O}C. The shaded area

between two such solutions indicates the lo-

cations of velocity profiles for intermediate

T_∞ values. These profiles are based on the

elastic properties of pure dry olivine

(Kumazawa and Anderson, 1969) and are calculated

from the geotherms for dry olivine, $u_o =$

2 cm/yr (solid lines). The dashed lines are

profiles for $T_\infty = 1200$ ^{O}C, $u_o = 10$ cm/yr and

$V* = 30$ cm^3/mole. For 10 My, the dashed lines

coincide with the $T = 1200$ ^{O}C solid lines.

Figure 17. Comparison of geotherms based on simple

boundary layer cooling for 10 My and 150 My

and $T_\infty = 1200$ ^{O}C and 1600 ^{O}C, with various

solidus curves. a - dry solidus; b - solidus

in presence of hydrated minerals; c - wet

solidus. These three solidi are from Kushiro

et al. (1968). The dashed solidus is that of

Ito and Kennedy (1967) for dry peridotite.

ridge

$T = T_O$, $u = u_O$, $v = 0$

topography, heat flow q_O

x

$T(x,y)$, $u(x,y)$, $v(x,y)$, $\tau(x)$

Lithosphere

viscosity, seismic velocities

y

v

u

Asthenosphere
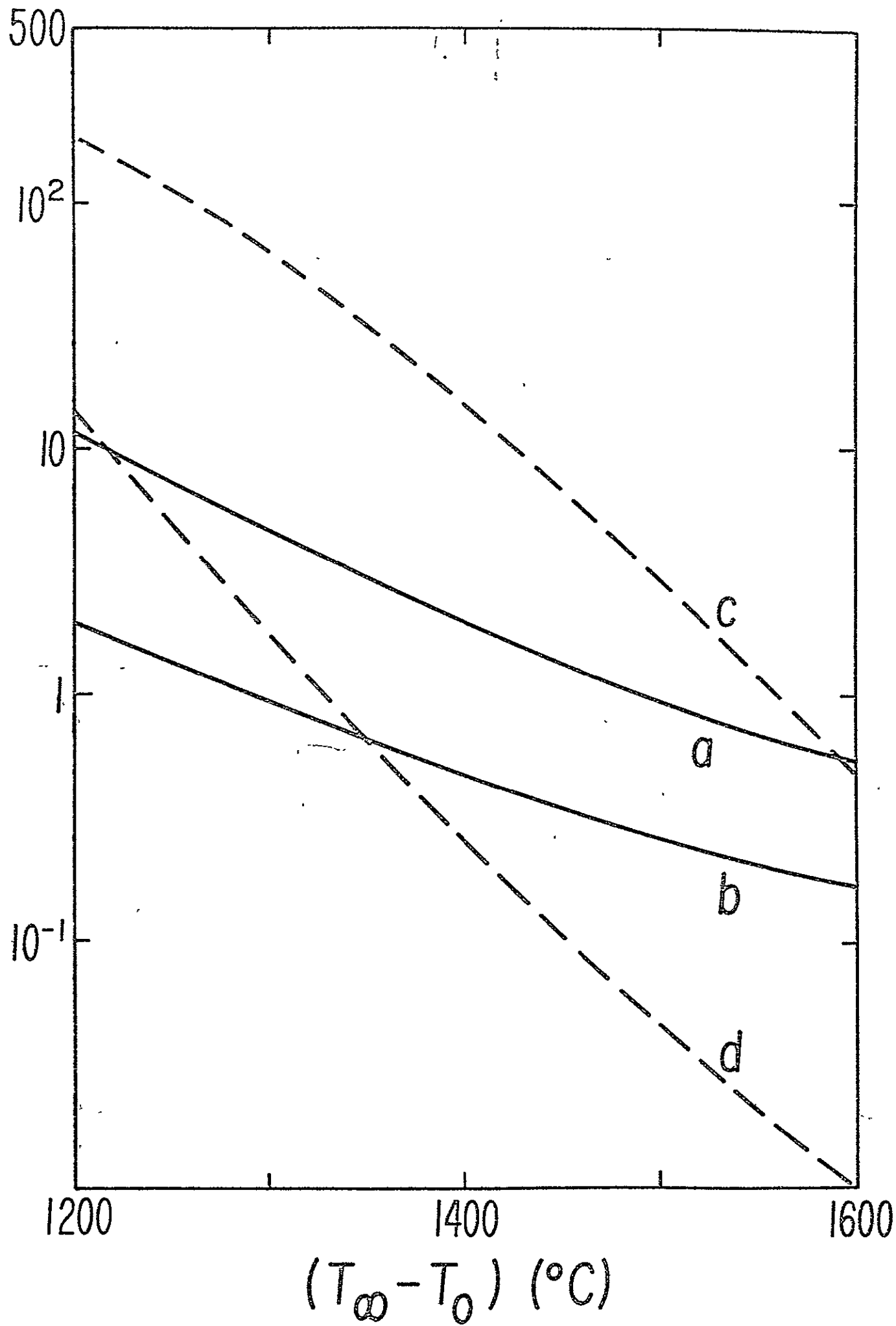
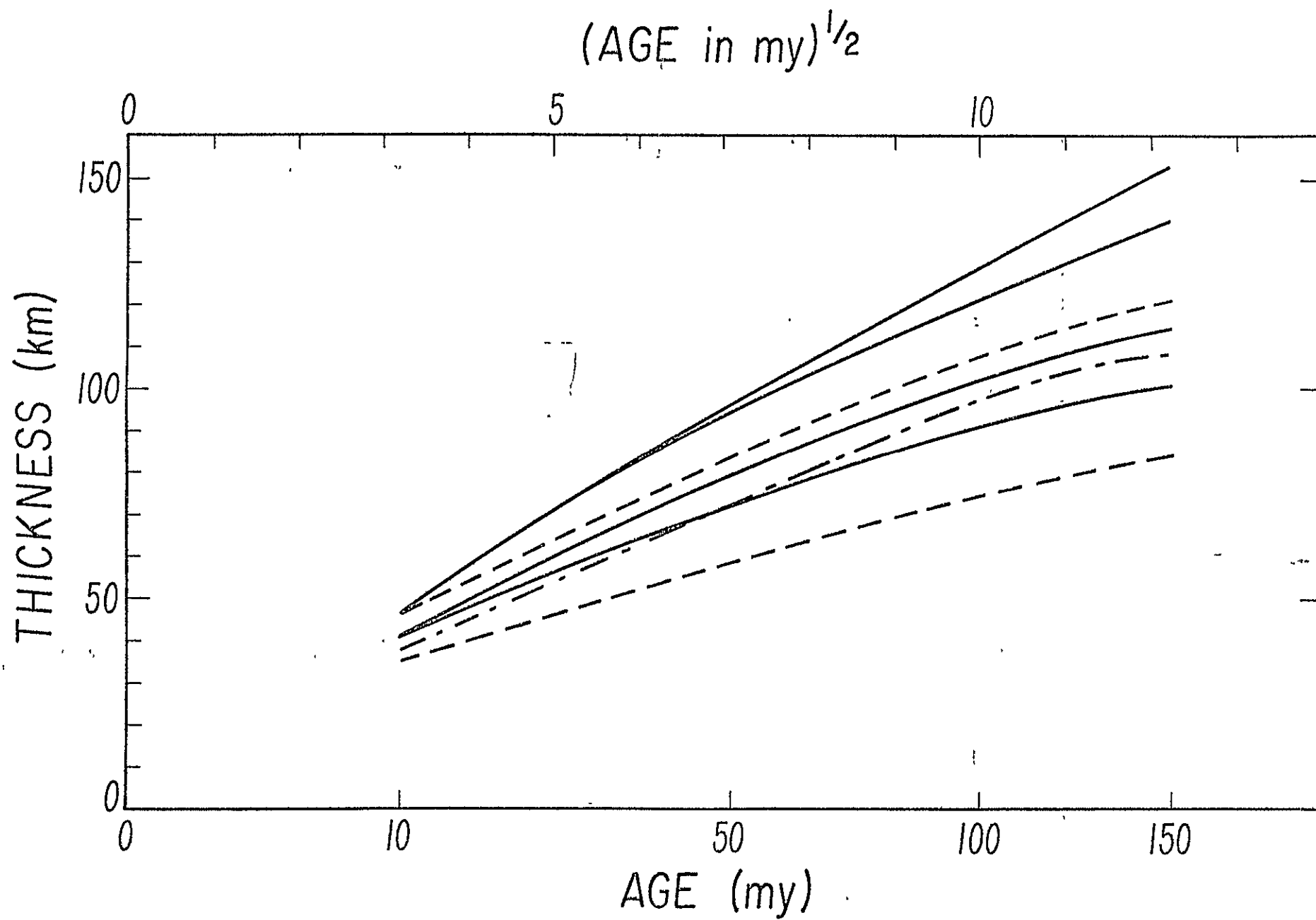$T = T_\infty$, $u = 0$

Fig. 1

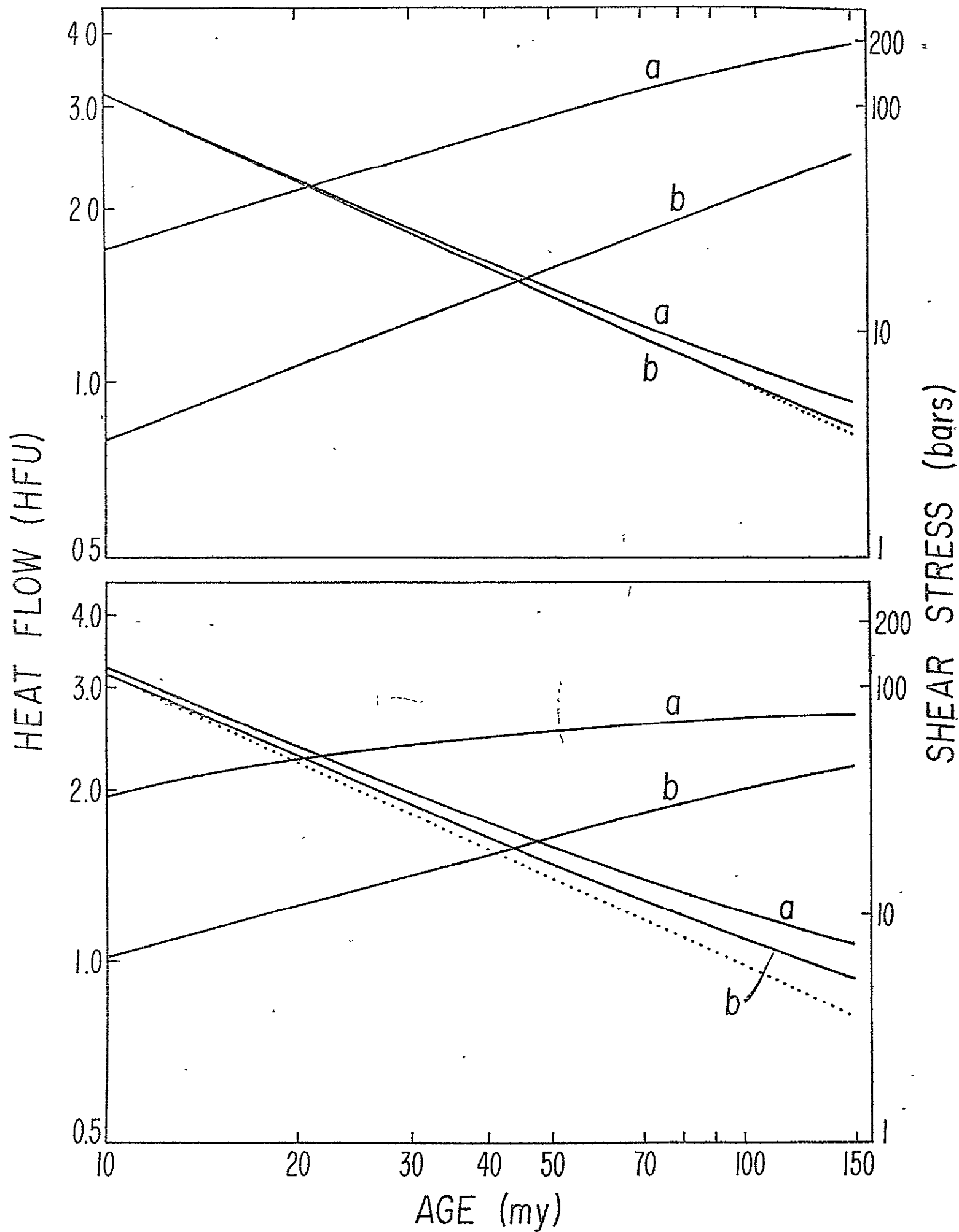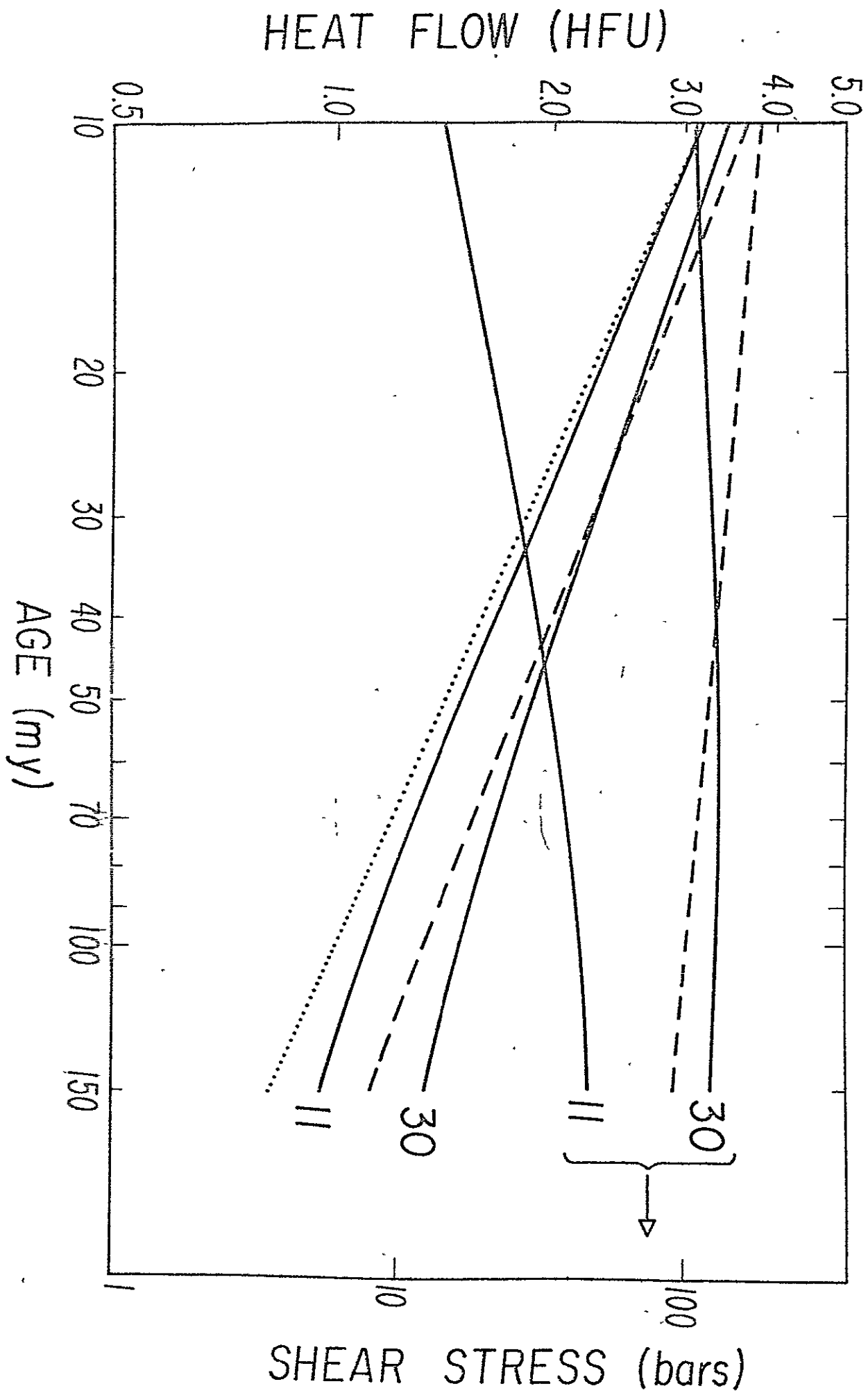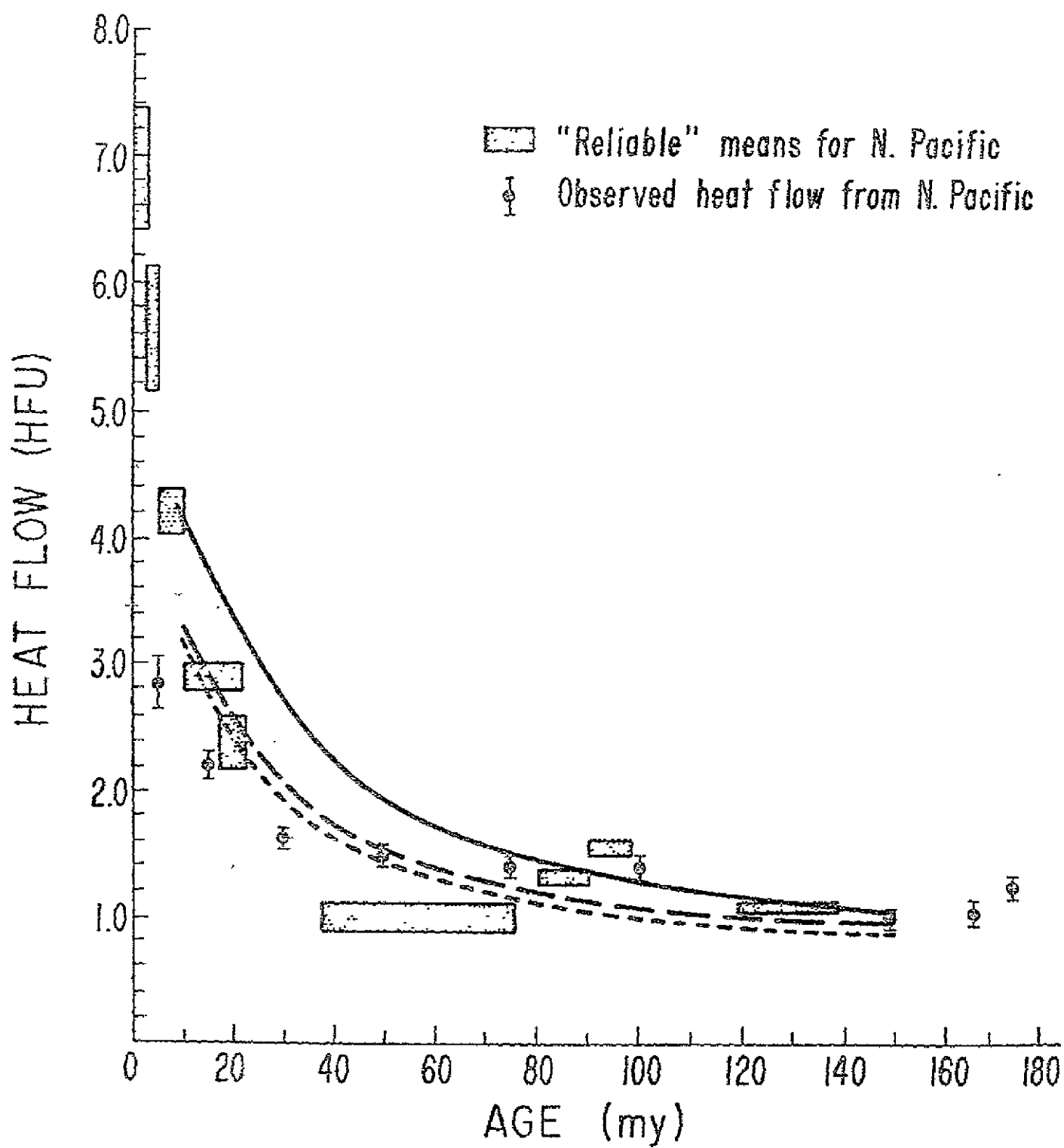Fig. 2

Fig. 3

Fig. 4

Fig. 5

Fig. 6

Fig. 7

Fig. 8

Fig. 9

Fig. 10

Fig. 11

Fig. 12

Fig. 13

Fig. 14

Fig. 15

Fig. 16

Fig. 17